

00004302861

Submitted to Applied Spectroscopy  
Reviews

LBL-3754  
Preprint (.)

RECEIVED  
LAWRENCE  
RADIATION LABORATORY

JUN 6 1975

LIBRARY AND  
DOCUMENTS SECTION

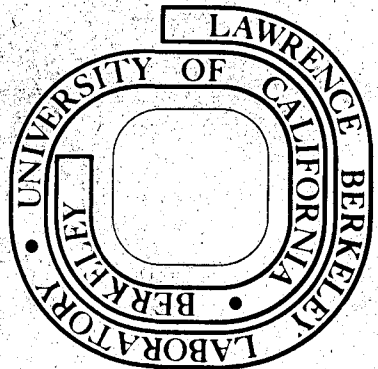
LASER EXCITATION MATRIX-ISOLATION SPECTROSCOPY

Lester Andrews

April 1975

Prepared for the U. S. Energy Research and  
Development Administration under Contract W-7405-ENG-48

**For Reference**  
Not to be taken from this room



LBL-3754  
(.)

## **DISCLAIMER**

This document was prepared as an account of work sponsored by the United States Government. While this document is believed to contain correct information, neither the United States Government nor any agency thereof, nor the Regents of the University of California, nor any of their employees, makes any warranty, express or implied, or assumes any legal responsibility for the accuracy, completeness, or usefulness of any information, apparatus, product, or process disclosed, or represents that its use would not infringe privately owned rights. Reference herein to any specific commercial product, process, or service by its trade name, trademark, manufacturer, or otherwise, does not necessarily constitute or imply its endorsement, recommendation, or favoring by the United States Government or any agency thereof, or the Regents of the University of California. The views and opinions of authors expressed herein do not necessarily state or reflect those of the United States Government or any agency thereof or the Regents of the University of California.

LASER EXCITATION MATRIX-ISOLATION SPECTROSCOPY

Lester Andrews\*

Inorganic Materials Research Division, Lawrence Berkeley Laboratory  
and Chemistry Department, University of California  
Berkeley, California 94720

received April 1975

to appear in

APPLIED SPECTROSCOPY REVIEWS

\*The author is a Sesquicentennial Associate on sabbatical leave from the  
University of Virginia, and an Alfred P. Sloan Fellow.

## INTRODUCTION

Perhaps the most significant recent development in the field of matrix isolation spectroscopy has proven to be the laser-Raman matrix technique. The complementary use of both infrared absorption and Raman scattering spectroscopic methods provides more complete vibrational data for the large body of interesting molecular species which require matrix synthesis and stabilization. The laser-excitation technique offers several advantages over the infrared experiment: the possibility of laser photolysis to create new chemical species, the observation of resonance-Raman spectra which provides harmonic and anharmonic vibrational constants from overtone bands, and the possible observation of fluorescence from new chemical species. Specific experimental examples of complementary infrared and Raman studies, laser photolysis, resonance-Raman, and fluorescence spectra will be discussed.

In a recent review of infrared and Raman spectra of unique matrix-isolated molecules, this author discussed the complementary use of infrared and Raman techniques for investigating matrix-isolated species (1). As a matter of historical interest, the first laser-Raman spectrum of a matrix-isolated species at high dilution in an inert matrix was reported by Shirk and Claassen for  $\text{SF}_6$  and  $\text{CHCl}_3$  (2). Early laser-Raman matrix-isolation studies employing a variety of techniques to produce interesting chemical species have been described by Ozin (3). Nibler has also discussed some of the initial matrix-Raman experiments in his laboratory (4). This review will describe some of the previous studies in the author's laboratory and new results from the last two years of research. First, a few comments on the several experimental techniques will be presented.

## EXPERIMENTAL

The details of infrared and Raman matrix isolation experiments have been described in several reviews (1,3,4) and manuscripts (5-7). Here, the sample deposition technique used for Raman studies will be discussed with particular attention to comparison with the infrared experiments.

Most laser-Raman matrix samples are deposited on tilted metal wedges from which the laser beam is scattered; OFHC copper, silver and aluminum are the most common block materials; near grazing angles of incidence of approximately  $10^\circ$  are commonly employed. Several major differences in infrared and Raman sample preparation are obvious. The infrared sample should be transparent to infrared radiation in general; deposition rates and window cleanliness are critical here; different deposition rates are sometimes required for producing transparent samples of different chemical systems. It is desirable to deposit transparent samples for infrared studies to maintain good signal-to-noise conditions and to allow examination of relatively thick samples which may be required for the observation of weak infrared bands. The Raman sample should be light in color for optimum light scattering. Obviously, dark samples will produce poor Raman scattering. It has been our experience that the most critical aspect of the Raman matrix experiment is sample deposition; visual monitoring of the sample during deposition is necessary for optimum sample preparation in these experiments. In general, less sample is required for the Raman experiment. Our Raman experiments require 4-6 hours of sample deposition (2 mmole/hour of gas deposited) whereas optimum infrared experiments require 18-24 hours. There is, of course, a practical limit to the laser penetration depth into the matrix sample, and laser beam heating of the sample surface will be more critical for thicker samples.

Laser power is an important parameter. Clearly, the minimum laser power for a good measurable signal is desirable, particularly for samples which may be photosensitive. We have observed the matrix isolated ozonide ion with 7 mW of 4880 Å excitation (this resonance Raman spectrum will be discussed in detail) (8), whereas approximately 700 mW of 4880 Å illumination was required to photoproduce OF and observe its Raman spectrum (9).

Frequencies can be measured more accurately in infrared than in the Raman experiments. Typical expanded scale, infrared slow-speed scans provide frequency accuracies of  $\pm 0.5 \text{ cm}^{-1}$ ; with great care and in-place calibration, very sharp bands may be measured to  $\pm 0.1 \text{ cm}^{-1}$ . Accurate Raman frequency shift measurements require superposition of plasma emission lines on the actual scan. This can be conveniently done by reducing the amplification and replacing the laser transmitting "spike" dielectric filter with a neutral density filter. Ideally, a Raman shifted band should be measured relative to nearby fluorescence lines on high and low frequency sides. This careful measurement allows Raman shifts to be recorded with  $\pm 0.5 \text{ cm}^{-1}$  accuracy. Five measurements of the OF fundamental in solid argon ranged from  $1028.6 \text{ cm}^{-1}$  to  $1029.2 \text{ cm}^{-1}$  (9); five measurements of  $\text{O}_2^-$  in the argon matrix isolated  $\text{Li}^+\text{O}_2^-$  species ranged from  $1096.0 \text{ cm}^{-1}$  to  $1097.1 \text{ cm}^{-1}$  (10).

Mercury arc photolysis has been widely used to photoproduce interesting new species for infrared spectral study. The Raman matrix technique conveniently provides a photolysis source, the laser excitation, for those molecules which undergo photolysis at the laser wavelength. The high power density of the laser beam makes photolysis practicable even for wavelengths

with low extinction coefficients. Laser photolysis of argon matrix isolated  $\text{OF}_2$  has produced observable quantities of OF from photodecomposition of a small fraction the  $\text{OF}_2$  precursor (9). In similar studies on  $\text{Cl}_2\text{O}$  in solid argon,  $\text{Cl}_2\text{O}$  Raman bands were observed along with the photolysis products ClO and ClClO (11). Raman studies of argon matrix isolated ozone showed a slow, continual photolysis of ozone as evidenced by growth of  $\text{O}_2$  signal and decrease of  $\text{O}_3$  signal (12). For appropriately selected precursor molecules, the matrix appears to moderate the photolysis process allowing Raman spectra of both precursor and photolysis product molecules to be obtained. Photochemical synthesis of  $\text{XeCl}_2$  has been recently accomplished with blue laser light on xenon-chlorine mixtures (13). The wide range of excitation wavelengths found in the argon and krypton plasma lasers can be used to great advantage in photolysis of matrix isolated molecules.

The matrix also provides a suitable host medium for the observation of resonance Raman spectra. Photodecomposition of the matrix-isolated ozonide ion was moderated sufficiently to allow observation of resonance Raman spectra using argon ion excitation (8), whereas examination of polycrystalline material at these wavelengths produced decomposition (14). The matrix reaction technique also provides new species for resonance Raman study. The alkali metal-iodine matrix reaction produced a new species identified as  $\text{M}^+\text{I}_2^-$  which required red excitation for resonance enhancement (15). In the case of gas phase  $\text{ClO}_2$ , laser excitation produced fluorescence (16); however, in an argon matrix host, quenching of fluorescence made possible the observation of the resonance Raman spectrum of  $\text{ClO}_2$  and fluorescence at appropriately spaced frequencies (17). The resonance fluorescence spectrum has been

observed for gaseous  $\text{NO}_2$  using 5145 and 4880 Å laser excitation (18). With these exciting wavelengths, argon matrix isolated  $\text{NO}_2$  exhibits a resonance Raman spectrum of the  $\nu_1$  and  $\nu_2$  fundamentals and several overtone bands (19).

Laser-induced fluorescence studies of matrix-isolated species also provide a wealth of chemical information. Recent studies on  $\text{C}_2^-$  in solid argon indicate vibrational lifetimes in the ms range (20). In argon and krypton plasma laser investigations of matrix-isolated carbenes, fluorescence progressions in  $\nu_1$  and  $\nu_2$  of  $\text{CCl}_2$  were observed (21). Sample dilution was a critical factor in these studies; reagent concentrations on the order of 0.1% were required to produce the best resolution of spectral features and to remove intermolecular perturbations.

We now turn our attention to a number of recent laser-excitation studies of matrix-isolated species.

RAMAN STUDIES OF ALKALI-METAL ATOM MATRIX REACTION PRODUCTS

Matrix Reactions with O<sub>2</sub>

Alkali metal atom-oxygen molecule matrix reactions have been extensively studied by this author and his coworkers using infrared and Raman techniques. The primary reaction yields the superoxide species which will be discussed in



detail. Two secondary reactions yield the peroxide species



and the disuperoxide species



In the first study of M-O<sub>2</sub> matrix reactions, this author reported a new chemical species, lithium superoxide Li<sup>+</sup>O<sub>2</sub><sup>-</sup>, with ionic bonding between Li<sup>+</sup> and O<sub>2</sub><sup>-</sup>, and an isocenes triangular structure (22). These conclusions were based upon the near agreement between the O-O mode for LiO<sub>2</sub> and the O<sub>2</sub><sup>-</sup> fundamental and the observation of sharp triplet bands in the reaction of <sup>16</sup>O<sub>2</sub>/<sup>16</sup>O<sup>18</sup>O/<sup>18</sup>O<sub>2</sub> with <sup>7</sup>Li atoms at high dilution in argon and a vibrational analysis involving six isotopic LiO<sub>2</sub> molecules. Figure 1 contrasts the infrared spectrum in this critical experiment with the Raman spectrum of a similar argon matrix sample (10).

First, examine the O<sub>2</sub><sup>-</sup> region near 1100 cm<sup>-1</sup>. The 1096.1 cm<sup>-1</sup> Raman band observed at 1096.6 cm<sup>-1</sup> in the infrared is due to <sup>7</sup>Li<sup>+</sup><sup>16</sup>O<sub>2</sub><sup>-</sup>; the 1065.7 cm<sup>-1</sup> Raman band recorded at 1066.5 cm<sup>-1</sup> in the IR is due to <sup>7</sup>Li<sup>+</sup><sup>16</sup>O<sup>18</sup>O<sup>-</sup>; the 1034.6 cm<sup>-1</sup> Raman signal measured at 1035.2 cm<sup>-1</sup> in the infrared is due to <sup>7</sup>Li<sup>+</sup><sup>18</sup>O<sub>2</sub><sup>-</sup>. The large 61 cm<sup>-1</sup> oxygen isotopic shift indicates the pure

oxygen character of this vibration, which is identified as  $\nu_1$ , the intraionic  $(O \leftrightarrow O)^-$  mode. The central feature reveals the molecular structure. In both infrared and Raman experiments, the single 16-18 isotopic band was sharp, just as sharp as the 16-16 and 18-18 isotopic bands. This indicates that the 16-18 isotope produces a single molecular arrangement  $M_{18}^{16}$  with equivalent oxygen atoms, in contrast to two possible M-16-18, M-18-16 arrangements which would be expected to produce a split central band as was observed for  $H^{16}O^{18}O$  and  $H^{18}O^{16}O$  (23). In the infrared experiments, this band was very sharp,  $1.0 \text{ cm}^{-1}$  half-width. It appears that  $0.2 \text{ cm}^{-1}$  is a reasonable upper limit on the inequivalence of the O atoms in  $Li^+O_2^-$  in the  $Li^{+16}O^{18}O^-$  isotopic band.

Second, in the Li-O stretching region, two intense resolved triplet bands were observed in the infrared, a single **broader**, weaker feature was observed in the Raman spectrum. The large lithium isotopic shift and smaller oxygen isotopic shift indicate that the band near  $700 \text{ cm}^{-1}$  is the symmetric interionic mode  $\nu_2$ ,  $Li^+ \leftrightarrow O_2^-$ , and the smaller lithium isotopic shift and larger oxygen isotopic shift show that the band near  $500 \text{ cm}^{-1}$  is  $\nu_3$ , the antisymmetric interionic mode. The G-matrix elements for these normal modes weight the participation of Li and O atoms differently (22).

Comparison of band intensities in Figure 1 also reflects on the bonding in the  $Li^+O_2^-$  species. The infrared spectrum shows a weak intraionic mode,  $\nu_1$ , and very intense interionic modes,  $\nu_2$  and  $\nu_3$ , as would be expected for an ionic model. The Raman spectrum contains a very intense intraionic mode  $\nu_1$ , a moderately intense symmetric interionic mode  $\nu_2$  and the antisymmetric interionic mode  $\nu_3$  is absent. The ionic model for  $LiO_2$  is supported by the complementary Raman spectrum.

The heavier alkali metals Na, K, Rb, and Cs react with oxygen to produce the superoxide  $M^+O_2^-$  species (24,25,26). Raman spectra for the Na, K, Rb, and Cs atom- $O_2$  reactions show a strong band near  $1110\text{ cm}^{-1}$  for the  $O_2^-$  vibration (27,28). The infrared spectra are typified by Cs atom cocondensation spectra with four isotopic oxygen samples (26). The very sharp, weak infrared band at  $1115.6\text{ cm}^{-1}$  has a strong Raman counterpart at  $1114\text{ cm}^{-1}$ . Isotopic substitution shows that this is the  $\nu_1 O_2^-$  intraionic fundamental in a  $Cs^+O_2^-$  species with two equivalent oxygen atoms. The very intense bands near  $230\text{ cm}^{-1}$  and weak bands at  $260\text{ cm}^{-1}$  are the interionic  $\nu_2$  and  $\nu_3$  modes, respectively, of  $Cs^+O_2^-$ .

The  $Cs^+O_2^-$  vibrational data are contrasted in Table I with frequencies for the other  $M^+O_2^-$  molecules. Note the increase in  $\nu_1$  with increasing cation size. This trend has been rationalized (10) as follows: increasing the cation polarizability increases the induced dipole moment on the cation which is opposite in sense to the ion dipole; accordingly, a small amount of antibonding electron density is removed from  $O_2^-$  increasing the fundamental frequency in the direction of the  $O_2$  value ( $1552\text{ cm}^{-1}$ ). Also, note the larger decrease in  $\nu_2$  and smaller decline in  $\nu_3$  with increasing alkali atomic weight which is required by the G-matrix elements for these normal modes.

The peroxide species,  $M^+O_2^{2-}M^+$ , has been observed for the five alkali metals. Intense antisymmetric Li-O stretching bands at  $796$  and  $446\text{ cm}^{-1}$  for the  $^7\text{Li}$  species showed isotopic splittings appropriate for a species containing two equivalent lithium atoms and two equivalent oxygen atoms. A rhombus structure with an O-O bond was suggested for the  $M^+O_2^{2-}M^+$  molecule (22). In the heavier species, the sodium frequency counterparts were observed at  $525$  and  $254\text{ cm}^{-1}$  (24), and the upper band only was observed for

TABLE I

Fundamental Frequencies ( $\text{cm}^{-1}$ ) Assigned to the  $\nu_1$  Intraionic and  $\nu_2$  and  $\nu_3$  Interionic Modes of the  $C_{2v}$  Alkali Metal Superoxide Molecules in Solid Argon at 15 K

<u>Molecule</u>	<u><math>\nu_1</math></u>	<u><math>\nu_2</math></u>	<u><math>\nu_3</math></u>
${}^6\text{LiO}_2$	1097.4	743.8	507.3
${}^7\text{LiO}_2$	1096.9	698.8	492.4
$\text{NaO}_2$	1094	390.7	332.8
$\text{KO}_2$	1108	307.5	---
$\text{RbO}_2$	1111.3	255.0	282.5
$\text{CsO}_2$	1115.6	236.5	268.6

the K, Rb, and Cs species at 433, 389, and 357  $\text{cm}^{-1}$  (25,26).

The disuperoxide species,  $\text{M}^+\text{O}_4^-$ , have been observed for the heaviest alkali metals. The small lithium ion apparently is not large enough to stabilize the large  $\text{O}_4^-$  anion. The new  $\text{MO}_4$  species was first observed in K and Rb studies which produced extraordinarily intense, very sharp, bands at 993.4 and 991.7  $\text{cm}^{-1}$ , respectively (25). The cesium counterpart at 1002.5  $\text{cm}^{-1}$  illustrates the isotopic behavior of the new species; the intense new band shifted to 946.5  $\text{cm}^{-1}$  in the  $^{18}\text{O}_2$  reaction. The stoichiometry of the new species is revealed by the mixed isotopic reactions; the  $^{16}\text{O}_2 + ^{18}\text{O}_2$  sample produced a symmetric triplet at 1002.0, 970.2, and 946.5  $\text{cm}^{-1}$ , which indicates the presence of two equivalent  $\text{O}_2$  molecules in the new species. A well-resolved sextet was produced in the scrambled oxygen isotopic experiment. The explicit interpretation of the sextet indicates a species with equivalent  $\text{O}_2$  units with equivalent O atoms in each unit. Accordingly, a  $\text{D}_{2d}$  structure was first proposed by this author for the  $\text{O}_2\text{KO}_2$  species (25). Subsequently, Jacox and Milligan pointed out the existence of the  $\text{O}_4^-$  ion in ion-molecule reactions and suggested the  $\text{O}_4^-$  arrangement (29). Possible  $\text{O}_4^-$  anion arrangements and  $\text{M}^+$  cation positions have been explored by CNINDO calculations; "puckered five-membered ring"  $\text{M}^+\text{O}_4^-$  structure was suggested in which the two  $\text{O}_2$  parts of  $\text{O}_4^-$  are equivalent but the inequivalence in atomic positions for each  $\text{O}_2$  unit, which would be small spectroscopically, was not resolved in the infrared spectrum (26). The  $\text{O}_4^-$  anion was suggested to contain two "superoxide" bonds and a weak intermolecular bond between the two  $\text{O}_2$  units. A very strong Raman band near 300  $\text{cm}^{-1}$  for the  $\text{K}^+\text{O}_4^-$ ,  $\text{Rb}^+\text{O}_4^-$ , and  $\text{Cs}^+\text{O}_4^-$  species was assigned to this symmetric intermolecular mode  $(\text{O}_2 \leftrightarrow \text{O}_2)^-$ ; interpretation of this low-frequency

Raman band requires a very weak oxygen bond which is provided by the  $O_4^-$  anion in the  $M^+O_4^-$  species (28). The presence of the cation certainly influences the geometry of the  $O_4^-$  anion in the  $M^+O_4^-$  ion-pair.

#### Matrix Reactions with Ozone

Extensive infrared and Raman studies of matrix-isolated isotopic ozone molecules have been conducted by Andrews and Spiker (12). Here isotopic ozones ( $^{16}O_3$ ,  $^{18}O_3$ , and  $^{16,18}O_3$ ) were synthesized by tesla coil discharge of  $O_2$  gas in a pyrex finger immersed in liquid nitrogen.

Oxygen was outgassed from the blue, liquid ozone sample by evacuating the sample at 77 K. Argon/ozone samples were prepared using standard (careful!) manometric techniques in a stainless steel vacuum system.

Matrix reactions of alkali metal atoms and ozone have also been studied using infrared and Raman methods. The infrared spectra (30) were characterized by very intense bands near  $800\text{ cm}^{-1}$  depending upon the alkali atom and the weaker bands near  $600\text{ cm}^{-1}$  for the heavier alkali metal reactions. The intense  $800\text{ cm}^{-1}$  bands were assigned to  $\nu_3$  and the weak  $600\text{ cm}^{-1}$  bands were attributed to  $\nu_2$  of  $O_3^-$  in the  $M^+O_3^-$  species, produced by charge-transfer reaction (4).



The cesium atom-ozone reaction produced intense  $\nu_3$  bands at 802 and  $757\text{ cm}^{-1}$  for  $Cs^{+16}O_3^-$  and  $Cs^{+18}O_3^-$ , respectively, and weaker  $\nu_2$  bands at 600 and 567 for the same respective isotopic species. In addition, oxygen atom abstraction was evidenced by observation of  $Cs_2O$  at  $457\text{ cm}^{-1}$  and  $CsO$  at  $322\text{ cm}^{-1}$  (30).

Sample preparation for Raman scattering experiments was closely monitored using white light; formation of the  $M^+O_3^-$  species was evidenced by the appearance of the orange ozonide color (8). Great care must be taken to prevent excess alkali metal which produces darker, and, thus, poorer scattering samples. Figure 2 illustrates the Raman spectra of Na- $O_3$  matrix reactions (8). A very intense Raman band was observed at  $1011\text{ cm}^{-1}$  with a site splitting at  $1024\text{ cm}^{-1}$  in the  $Na^{+16}O_3^-$  spectrum. Large oxygen-18 shifts are indicated by the  $Na^{+18}O_3^-$  spectrum; the intense band and site splitting shifted to  $956$  and  $970\text{ cm}^{-1}$ , respectively. The  $Na^{+16,18}O_3^-$  Raman spectrum shows five well-resolved components, the broader central component contains both 16-18-16 and 18-16-18 isotopic species. A five-component multiplet with the same relative intensities has been observed for  $\nu_1$  of matrix-isolated 55% oxygen-18 enriched ozone (12). As was the case for  $\nu_3$  of  $O_3$  and  $O_3^-$  in the infrared spectra (30),  $\nu_1$  of  $O_3$  and  $O_3^-$  produced similar isotopic bands in the Raman spectra.

The weak band at  $599\text{ cm}^{-1}$  in the  $Na^{+16}O_3^-$  Raman spectrum has an ozone-18 counterpart at  $567\text{ cm}^{-1}$ ; individual isotopic components were not resolved in the  $^{16,18}O_3$  reaction. These features are in good agreement with the infrared assignments to  $\nu_2$  of  $O_3^-$  in the cesium species (30); accordingly, the weak Raman bands were assigned to  $\nu_2$  of  $O_3^-$  in the sodium ozonide molecule (8).

The very intense fundamental Raman bands for the ozonide species and the deep orange sample color prompted a search for overtones of the  $\nu_1$  fundamental. An electronic absorption band with vibrational fine structure in the  $5100\text{-}3700\text{ \AA}$  region has been observed by Jacox and Milligan (31) and this author (32) for  $O_3^-$  in the  $M^+O_3^-$  species. Accordingly,  $4880\text{ \AA}$  laser excitation of matrix-isolated  $Cs^+O_3^-$  yielded

a regular progression of fundamental and overtone bands at 1018, 2028, 3024, and 4014  $\text{cm}^{-1}$  with regularly decreasing intensities. The  $\text{Cs}^{+18}\text{O}_3^-$  species produced a progression out to  $5\nu_1$ ; bands were observed at 962, 1915, 2859, 3795, and 4724  $\text{cm}^{-1}$  (8). The regularly decreasing intensity pattern for an overtone progression is characteristic of the resonance Raman effect.

Figure 3 contrasts the use of six different laser exciting lines on the Raman spectrum of  $\text{Na}^+\text{O}_3^-$ . The 6471 Å line produced a weak fundamental at 1011  $\text{cm}^{-1}$  on a steep fluorescence background. 5682 Å excitation gave an intense fundamental at 1011  $\text{cm}^{-1}$  and a weak first overtone at 2013  $\text{cm}^{-1}$ . The 5309 Å line produced an intense fundamental at 1012  $\text{cm}^{-1}$ , a first overtone at 2013  $\text{cm}^{-1}$  and a weak second overtone at 3001  $\text{cm}^{-1}$ . 5145 Å excitation yielded the intense 1011  $\text{cm}^{-1}$  fundamental, intense first and second overtones at 2013 and 3002  $\text{cm}^{-1}$  and a weak third overtone at 3977  $\text{cm}^{-1}$ ; the 4880 Å line produced the intense fundamental and two intense overtones at the same frequencies. Figure 3 concludes with the 4579 Å exciting line which gave the intense fundamental and two moderately intense overtones (8). Clearly, the overtone intensity is enhanced as the excitation wavelength approaches the electronic absorption band maximum. This increase in overtone intensity relative to fundamental intensity as the exciting wavelength enters the electronic band is characteristic of resonance Raman spectra.

Analysis of the overtone progressions for the  $\text{Cs}^{+16}\text{O}_3^-$  species produced the vibrational constants  $\omega_1 = 1028.2 \pm 1.0 \text{ cm}^{-1}$  and  $x_{11} = 4.95 \pm 0.25 \text{ cm}^{-1}$ . The harmonic and anharmonic vibrational constants provide a measure of the heat of atomization,  $\text{O}_3^- \rightarrow 2\text{O} + \text{O}^-$ , of the ozonide ion using a linear

Birge-Spooner extrapolation to the dissociation limit. The spectroscopic heat of atomization,  $153 \pm 3$  kcal/mole, agrees well with the thermodynamic value, and it provides an independent check on the electron affinity of ozone (8).

The present Raman spectra for the  $M^+O_3^-$  species demonstrate the usefulness of the matrix reaction technique to produce and stabilize observable quantities of unstable species for laser examination. The ozonide Raman fundamentals near  $1010 \text{ cm}^{-1}$  in the matrix isolation study agree with He-Ne observations on polycrystalline ozonides (14) and very recent resonance Raman studies of  $O_3^-$  produced by  $\gamma$ -radiolysis of  $KClO_3$  crystals (33). The matrix host moderates the photodecomposition of the  $M^+O_3^-$  molecule, quenches fluorescence and allows the resonance Raman spectrum of  $O_3^-$  to be observed using argon ion excitation.

#### Alkali Metal-Fluorine Reaction Products

Fluorine was the first halogen molecule to be studied in alkali metal matrix reactions owing to the presence of a  $475 \text{ cm}^{-1}$  Raman band in sodium- $OF_2$  studies which showed no oxygen-18 shift (34). Matrix samples prepared by codepositing Na atoms with argon containing 1%  $F_2$  exhibited a strong Raman band at  $475 \text{ cm}^{-1}$  and a weaker band at  $892 \text{ cm}^{-1}$  due to  $F_2$  using  $4880 \text{ \AA}$  laser excitation (35,36). The  $475 \text{ cm}^{-1}$  scattering species was photosensitive; the signal had a half-life of approximately 10 min. Matrix reactions of Li, K, Rb, and Cs with  $F_2$  were performed and the new Raman bands observed near  $460 \text{ cm}^{-1}$  are listed in Table II.

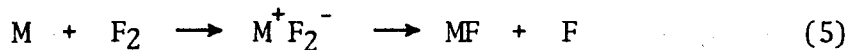
TABLE II

Fundamental Frequencies ( $\text{cm}^{-1}$ ) Assigned to the  $\nu_1$  Intraionic ( $X \leftrightarrow X$ )<sup>-</sup>  
Mode of the  $M^+X_2^-$  Species Observed in Matrix Raman Spectra

	$F_2^-$	$Cl_2^-$	$I_2^-$
$Li^+$	452	246	115
$Na^+$	475	225	114
$K^+$	464	264	113
$Rb^+$	462	260	116
$Cs^+$	459	259	115

Figure 4 contrasts Raman spectra of fluorine-chlorine and sodium matrix reaction products. The top spectrum shows the 475  $\text{cm}^{-1}$  band from the reaction with  $\text{F}_2$  and the bottom spectrum, to be described fully in the next section, exhibits  $\text{Cl}_2$  signal at 538  $\text{cm}^{-1}$ , a weak band at 275  $\text{cm}^{-1}$  and a strong signal at 225  $\text{cm}^{-1}$ , the latter of which is due to  $\text{Cl}_2^-$  in the  $\text{Na}^+\text{Cl}_2^-$  species. The middle trace shows the Raman spectrum of a mixed  $\text{F}_2\text{-Cl}_2$  reaction; only two dominant product signals were noted and these appeared at 475 and 225  $\text{cm}^{-1}$ , the same positions observed in the  $\text{F}_2$  and  $\text{Cl}_2$  runs, respectively. This indicates that the scattering species contains two halogens, and therefore, the formula must be  $\text{M}^+\text{X}_2^-$ .

It is proposed that  $\text{F}_2^-$  was formed as an intermediate in reaction (5) which goes completely in some cases, but the  $\text{M}^+\text{F}_2^-$  "collision complex" is stabilized by the matrix in sufficient quantities for laser Raman detection.



Photodecomposition of  $\text{M}^+\text{F}_2^-$  probably proceeds to the more thermodynamically stable MF and F products.

The Raman signals for the  $\text{M}^+\text{F}_2^-$  species are assigned to the intraionic  $(\text{F-F})^-$  vibration. Their appearance at approximately half of the  $\text{F}_2$  fundamental is in qualitative agreement with molecular orbital theory for diatomic molecules which predicts a one-half bond order for  $\text{F}_2^-$ . The alkali metal shift on the  $\text{F}_2^-$  wavenumbers arises from interaction between the interionic  $\text{M}^+\leftrightarrow\text{F}_2^-$  vibration and the  $(\text{F}\leftrightarrow\text{F})^-$  mode; the former, is of course, very sensitive to the alkali mass. The  $\text{M}^+\text{O}_2^-$  species provide a guide as to the expected positions of the interionic modes; a cross-over occurs between Li and Na with the  $\text{F}_2^-$  mode. Interionic modes for  ${}^6\text{Li}^+\text{-F}_2^-$  and  $\text{Na}^+\text{-F}_2^-$  have been

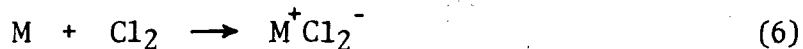
identified at 708 and 454  $\text{cm}^{-1}$  in infrared studies (36). Interaction between the higher-frequency lithium-stretching and  $(\text{F-F})^-$  stretching modes forces the latter to a lower frequency, whereas the heavier sodium interionic mode shifts below the  $\text{F}_2^-$  mode and forces  $\text{F}_2^-$  to a higher frequency. Increasing the mass to K, Rb, and Cs removes the interaction, and the  $\text{F}_2^-$  mode appears near 460  $\text{cm}^{-1}$ .

An optical absorption study of alkali metal atom-halogen molecule reaction products is in progress (37). A very strong absorption at 310 nm was produced in the Na- $\text{F}_2$  reaction; this band was photobleached by a tungsten lamp. The 310 nm optical band is believed due to  $\text{F}_2^-$ ; its appearance to the long wavelength of  $\text{F}_2$  at 284.5 nm (38) is noted.

#### Alkali Metal-Chlorine Reaction Products

Matrix reactions of chlorine and alkali metal atoms produced extraordinarily intense Raman signals in the 225-260  $\text{cm}^{-1}$  shifted region. Owing to the orange color of these matrix samples, resonance enhancement of the intensity was suspected and intense overtone series were noted with argon ion laser lines (39,40).

Figure 5 contrasts the Raman spectra of the five alkali metal products of reaction (6). Note the very intense fundamentals, ranging from 264  $\text{cm}^{-1}$



for  $\text{K}^+\text{Cl}_2^-$  to 225  $\text{cm}^{-1}$  for  $\text{Na}^+\text{Cl}_2^-$  which show a clear alkali metal trend as listed in Table II. These signals are assigned to the intraionic  $(\text{Cl-Cl})^-$  mode, and the alkali metal dependence is believed to be due to interaction

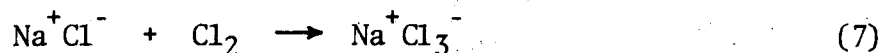
with the interionic  $M^+ \leftrightarrow Cl_2^-$  stretching mode which is predicted higher in the  $Na^+ Cl_2^-$  case, forcing the  $(Cl-Cl)^-$  mode down to  $225\text{ cm}^{-1}$ , and in the  $K^+ Cl_2^-$  species, the interionic mode is predicted at  $200\text{ cm}^{-1}$  forcing the  $(Cl-Cl)^-$  vibration up to  $264\text{ cm}^{-1}$ .

Figure 6 shows the extensive overtone series observed for the  $Cs^+ Cl_2^-$  species using  $4579\text{ \AA}$  laser excitation. Notice the resolution of natural chlorine isotopes in the overtones; the observed 9/6 intensity ratio for the upper two bands in each member of the progression for the (35-35) and (37-35) isotopic species confirms the presence of two equivalent chlorine atoms. The fundamental and first three overtones for the (37-37) isotopic species were observed using a  $^{37}Cl_2$  sample (40).

Standard wavenumber plots of the overtone data produce an excellent straight-line fit and the vibrational constants  $\omega_e = 262.1 \pm 0.3\text{ cm}^{-1}$  and  $\omega_e x_e = 1.55 \pm 0.07\text{ cm}^{-1}$  for  $Cl_2^-$  in the  $Cs^+ Cl_2^-$  species. It is also of interest that the upper limit to the  $(Cl-Cl)^-$  dissociation energy calculated from the harmonic and anharmonic vibrational constants,  $31.8\text{ kcal/mole}$ , is in very good agreement with the  $28.8 \pm 2.5\text{ kcal/mole}$  thermochemical value (40).

The optical absorption of  $Cl_2^-$  in the  $Cs^+ Cl_2^-$  species produced a band at  $350\text{ nm}$  (37). Figure 7 contrasts the Raman spectra of this species using  $514.5, 488.0, 476.5,$  and  $457.9\text{ nm}$  excitation. As the laser wavelength approached the absorption band maximum, intensity enhancement of the fundamental and overtone series was noted (40).

The intense Raman signal at  $275\text{ cm}^{-1}$  in the  $Na-Cl_2$  reaction spectrum of Figure 5 is due to  $\nu_1$  of  $Cl_3^-$  in the  $Na^+ Cl_3^-$  species.  $NaCl$  molecules, also produced in the cocondensation reaction and identified by an intense infrared band at  $335\text{ cm}^{-1}$  (40), react with  $Cl_2$  to produce  $Na^+ Cl_3^-$ , reaction (7).



This assignment has been confirmed by salt-molecule matrix reactions where NaCl and Cl<sub>2</sub> have been codeposited in solid argon (41).

#### Alkali Metal-Iodine Reaction Products

Matrix reactions of alkali metal atoms and iodine provide a particularly interesting chemical system for laser-Raman study. Using the potassium-iodine reaction products for the purpose of discussion, a very strong resonance Raman progression beginning at 113 cm<sup>-1</sup> with five overtones decreasing in intensity was observed using 6471 Å excitation. The 5682 and 5309 Å lines produced only a weak fundamental, and no signal was detected with 5145 Å excitation. However, when the 4880, 4579, and 3507 Å laser lines were used, an increasingly strong fundamental was observed near 112±2 cm<sup>-1</sup> (15).

The triiodide ion absorbs strongly at 294 and 364 nm in the near ultraviolet (42), and Raman spectra of I<sub>3</sub><sup>-</sup> in solution have been observed using blue and ultraviolet laser lines (43). However, I<sub>3</sub><sup>-</sup> has no absorption in the red visible region. It was proposed that the red-enhanced-intensity scattering species was I<sub>2</sub><sup>-</sup> produced by reaction (8). Reactions (9) and (10)



suggest a mechanism to produce I<sub>3</sub><sup>-</sup> which is responsible for the matrix Raman signals stimulated by blue and uv laser lines. The I<sub>2</sub><sup>-</sup> fundamentals

were a several  $\text{cm}^{-1}$  function of  $\text{M}^+$ , which arises from the  $\text{M}^+ \leftrightarrow \text{I}_2^-$  stretching interaction with the  $(\text{I-I})^-$  mode. The  $\text{M}^+ \text{I}_2^-$  Raman wavenumbers are also listed in Table II.

In optical absorption work in progress, the sodium-iodine matrix reaction produced strong bands at 380 nm for  $\text{Na}^+ \text{I}_3^-$  and 695 nm for  $\text{Na}^+ \text{I}_2^-$  (37) which supports the resonance Raman observation of  $\text{I}_2^-$  in the matrix reaction product  $\text{M}^+ \text{I}_2^-$  (15).

## LASER PHOTOLYSIS RAMAN STUDIES

## The OF and ClO Free Radicals

The oxygen fluoride free radical was first observed by Arkell and co-workers (44) following the mercury-arc photolysis of argon-OF<sub>2</sub> samples at 4 K. The matrix reactions of OF<sub>2</sub> and Li, Na, K, and Mg atoms were studied by Andrews and Raymond. The intense, sharp OF fundamental was observed at  $1028.6 \pm 0.3 \text{ cm}^{-1}$ , independent of the metal reagent; metal fluoride molecules were observed for all reagent metals (45).

The sodium-OF<sub>2</sub> matrix reaction was examined using the Raman matrix technique; a weak band at  $1028 \text{ cm}^{-1}$  was observed; however, it was noticed that the  $1028 \text{ cm}^{-1}$  band grew during the laser illumination period (34). The Raman spectrum of argon matrix-isolated OF<sub>2</sub> without alkali metal atoms is illustrated in Figure 8 (a); the sharp OF<sub>2</sub> fundamental bands  $\nu_2$  and  $\nu_3$  are noted at 464 and  $825 \text{ cm}^{-1}$  along with the Fermi doublet  $\nu_1$ ,  $2\nu_2$  at 920,  $931 \text{ cm}^{-1}$  (9). These frequencies are within one  $\text{cm}^{-1}$  of the infrared matrix assignments. Figure 8(a) also shows the laser photolytic production of the OF species. Note in the first trace, no signal was detected at  $1029 \text{ cm}^{-1}$  after 8 min of exposure to 700 mW of  $4880 \text{ \AA}$  excitation; however, after 25 min of laser illumination on the same spot of sample, a small signal appeared at  $1029 \text{ cm}^{-1}$  which grew to a strong signal after two hours of laser photolysis. Clearly, the  $1029 \text{ cm}^{-1}$  signal increased as a function of laser illumination time. In addition to the OF photolysis product, O<sub>2</sub> and F<sub>2</sub> were also observed at 1552 and  $892 \text{ cm}^{-1}$ , respectively. Accurate measurements of the OF fundamental frequency using argon emission lines superimposed on the actual scan yielded  $1028.9 \pm 0.5 \text{ cm}^{-1}$ , which is in excellent agreement with the infrared observations.

Figure 8(b) illustrates the Raman spectrum of an Ar/OF<sub>2</sub> = 100/1 sample deposited for four hours with simultaneous 4880 Å photolysis for the last three hours (9). Note the strong signals at 1029 cm<sup>-1</sup> and 892 cm<sup>-1</sup> for photolysis products of OF<sub>2</sub> and the strong signals for unphotolysed OF<sub>2</sub>. The matrix apparently moderates the laser photodecomposition of OF<sub>2</sub> such that excellent Raman spectra of precursor and photolysis products can be obtained.

The advantage of laser photolysis is demonstrated for OF<sub>2</sub>. The electronic transition for OF<sub>2</sub> photodecomposition increases in intensity with decreasing wavelength; the extinction coefficient is  $75 \times 10^{-5}$  at 2100 Å (46). Accordingly, the OF species was first observed by Arkell and co-workers following mercury arc photolysis of matrix isolated OF<sub>2</sub> (44). However, the OF<sub>2</sub> absorption tails out into the visible region with an extinction coefficient of  $0.14 \times 10^{-5}$  at 4880 Å. The high power density of the laser beam compensates for the low extinction coefficient at 4880 Å such that photolysis products of OF<sub>2</sub> are produced by laser illumination, and they can be identified by Raman spectra.

A similar laser-Raman study of Cl<sub>2</sub>O was done by Chi and Andrews (47). Figure 9 contrasts the 4880 Å excited Raman spectrum of 1% Cl<sub>2</sub>O in argon with the infrared spectrum of a similar sample subjected to 10 m of mercury arc photolysis. First, the stretching modes of Cl<sub>2</sub>O were observed in both spectra and, in addition,  $\nu_2$  was detected in the Raman spectrum. Rochkind and Pimentel previously identified the 962 and 375 cm<sup>-1</sup> infrared bands with a new photoisomer Cl-C1O (48). The Raman study confirmed their observation and added the Cl-Cl-O bending mode assignment of 239 cm<sup>-1</sup>. Perhaps of most interest is the direct Raman observation of the elusive ClO free radical

fundamental at  $850 \text{ cm}^{-1}$  which is in agreement with hot band spacings in the electronic spectrum (49).

#### Noble Gas Dihalides

The matrix isolation technique was employed in early infrared studies of  $\text{XeF}_2$  and  $\text{KrF}_2$  by Turner and Pimentel (50). Xenon dichloride was first identified by a  $313 \text{ cm}^{-1}$  infrared absorption arising from the condensed discharge products of xenon and chlorine (51); Raman studies on similar systems produced a  $253 \text{ cm}^{-1}$  band for  $\nu_1$  of  $\text{XeCl}_2$  (52). Owing to the appearance of this latter band in the  $\text{Cl}_2$  region, discussed in the previous section, and the possibility of trapping ions from discharge sources, photolytic methods of synthesizing  $\text{XeCl}_2$  were sought. Howard and Andrews (53) and, independently, Beattie and German (54), found that  $4880 \text{ \AA}$  laser irradiation of frozen samples of chlorine in xenon produced a strong Raman signal at  $254 \text{ cm}^{-1}$ . The observation of a 9/6/1 triplet (54) required two equivalent chlorine atoms in the scattering species and the energy available in blue light is sufficient to dissociate (and not ionize) molecular chlorine (53) which confirmed the identification of  $\text{XeCl}_2$ .

In a detailed wavelength study of laser photosynthesis of  $\text{XeCl}_2$ , Howard and Andrews found that production of the  $254 \text{ cm}^{-1}$  Raman signal was not possible with  $5145 \text{ \AA}$  light, was slow with  $5017 \text{ \AA}$ , rapid with  $4880 \text{ \AA}$ , and very rapid with  $4765 \text{ \AA}$  laser lines. The dissociation limit of  $\text{Cl}_2$  at  $4786 \text{ \AA}$  identifies the mechanism as the reaction of a photolytically produced pair of chlorine atoms with a xenon atom in the matrix cage (53).

In order to confirm this mechanism, xenon-fluorine and krypton-fluorine matrix samples were exposed to blue laser examination.  $\text{XeF}_2$  was produced immediately, as identified by a strong Raman band at  $512 \text{ cm}^{-1}$ ;  $\text{KrF}_2$  was synthesized more slowly, but a strong Raman band at  $452 \text{ cm}^{-1}$  was observed. Figure 10 contrasts the  $4880 \text{ \AA}$  laser synthesis of  $\text{XeF}_2$ ,  $\text{KrF}_2$ , and  $\text{XeCl}_2$  for Raman study. A similar laser photolysis experiment with krypton and chlorine failed to produce a new signal; however, microwave discharge of krypton and chlorine produced an extremely unstable signal at  $242 \text{ cm}^{-1}$  which was tentatively assigned to isolated  $\text{Cl}_3^-$  (53).

The mixed compound  $\text{XeClF}$  was reported by Howard and Andrews (53) using blue photolysis of  $\text{ClF}$  in solid xenon. Figure 11 contrasts the infrared and Raman spectra of  $\text{XeClF}$ . Note the strong  $480 \text{ cm}^{-1}$  and weak  $316 \text{ cm}^{-1}$  infrared bands and the appearance of these same signals in the  $4765 \text{ \AA}$  excited Raman spectrum. The  $480 \text{ cm}^{-1}$  infrared band was observed independently by Bondeybey and Pimentel following the condensation of excited xenon atoms with  $\text{ClF}$  diluted in argon (55). These compounds mark the limit of noble gas reactivity as attempts to prepare  $\text{KrCl}_2$  and  $\text{XeBr}_2$  met with no success (53).

## LASER EXCITATION STUDIES OF MOLECULAR HALOGENS

As supporting studies for the previously discussed matrix reactions of molecular halogens, a systematic laser excitation investigation of halogen molecules in matrices was undertaken in the Raman and fluorescence spectral regions.

Molecular fluorine at concentrations of 1 or 2% in solid argon produced a moderate  $892\text{ cm}^{-1}$  Raman signal using blue laser excitation, which is in agreement with the gas phase value and near the solid value (35,36). No fluorescence attributable to molecular fluorine was detected; however, a system of bands between  $14,000$  and  $19,000\text{ cm}^{-1}$  with a  $580\text{ cm}^{-1}$  spacing was observed with blue laser excitation of fluorine in argon, krypton, xenon, and nitrogen. This fluorescence is believed to be due to a metal fluoride arising from the reaction of fluorine with the vacuum system (56).

Raman and fluorescence spectra of matrix-isolated  $\text{Cl}_2$  depended upon concentration. Using 1 or 2%  $\text{Cl}_2$  in argon, a Raman band was observed at  $538\text{ cm}^{-1}$  (39) and a broad series of fluorescence bands appeared between  $11,000$  and  $15,000\text{ cm}^{-1}$  with a beginning spacing of approximately  $520\text{ cm}^{-1}$  when samples of  $\text{Ar}/\text{Cl}_2 = 300/1$  and more dilute were studied, a  $550\text{ cm}^{-1}$  Raman band and a sharp fluorescence series of 9/6/1 triplets between  $11,000$  and  $15,000\text{ cm}^{-1}$  were observed using  $5145$ ,  $4880$ ,  $4579$ , and  $3507\text{ \AA}$  laser lines. The latter sharp triplet fluorescence and  $550\text{ cm}^{-1}$  Raman band have been assigned to matrix isolated  $\text{Cl}_2$  and the series of broad fluorescence bands and  $538\text{ cm}^{-1}$  Raman signal have been attributed to aggregated chlorine. Agreement of the latter Raman band with the solid chlorine value was noted (57).

Laser excitation spectra of bromine in matrices followed the same pattern. For concentrations of 1%, a Raman fundamental at  $295\text{ cm}^{-1}$  and overtones at 586, 882, and  $1176\text{ cm}^{-1}$  were observed for aggregated bromine using  $4579\text{ \AA}$  excitation (58) along with a broad series of fluorescence bands. More dilute samples ( $\text{Ar}/\text{Br}_2 = 500/1$ ) gave resonance Raman bands of matrix isolated  $\text{Br}_2$  at 316, 629, 940, and  $1249\text{ cm}^{-1}$  and a fluorescence system from 10,500 to  $13,500\text{ cm}^{-1}$  which showed a beginning spacing of  $313\text{ cm}^{-1}$  and gave  $\omega_e = 317.5\text{ cm}^{-1}$  and  $\omega_{eXe} = 1.1\text{ cm}^{-1}$  for  $\text{Br}_2$  (57).

Molecular iodine proved even more difficult to matrix isolate, as the Raman spectra of Figure 12 indicate. At  $\text{Ar}/\text{I}_2 = 400/1$  a strong resonance Raman progression with a  $180\text{ cm}^{-1}$  fundamental dominates the spectrum. However, at  $\text{Ar}/\text{I}_2 = 2500/1$ , a strong resonance Raman series beginning at  $212\text{ cm}^{-1}$  is the only feature present. The agreement of these iodine fundamentals with the solid and gas phase values, respectively, denote the matrix-isolated scattering species as aggregated iodine and monomeric iodine (58).

It was found, as expected, that the more polarizable halogen molecules were more difficult to isolate as the diatomic molecule. Perhaps surprising was the fact that an iodine concentration of 1 part per 2500 matrix gas was required to eliminate the resonance Raman spectrum of aggregated iodine molecules.

In the fluorescence region, a relatively broad and strong fluorescence band with maxima at about  $16,600$  and  $15,700\text{ cm}^{-1}$  was observed with yellow, green, and blue laser lines (59). Since this broad fluorescence was observed under conditions where all of the resonance Raman signal was due

to monomeric iodine, the broad bands are believed due to  $I_2$  fluorescence broadened by matrix solvent effects.

Of special interest were two series of sharp fluorescence bands between 14,475-13,112 and 13,080-12,100  $\text{cm}^{-1}$  which appeared in almost all matrix studies of iodine. The two series had beginning spacings of 178 and 152  $\text{cm}^{-1}$  which increased out the fluorescence series showing a positive anharmonicity which can be explained by a new linear species of iodine. While the present information does not provide a basis for definitive identification of this linear iodine species, possibilities include transition metal diiodides such as  $\text{FeI}_2$  (60).

It is also possible to do meaningful quantitative intensity studies on matrix-isolated molecules. Grzybowski and Andrews (59) performed a laser excitation investigation of  $\text{TiI}_4$  at approximately 0.1% concentration in solid argon aimed at resonance Raman observation of  $\text{TiI}_4$  and found instead progressions in monomeric  $I_2$  out to  $\underline{\nu} = 25$ . Owing to the previously discussed strong tendency of  $I_2$  molecules to aggregate, the laser-induced decomposition of matrix-isolated  $\text{TiI}_4$  produced twice the concentration of isolated  $I_2$  that could be obtained with the element. High intensity resonance Raman overtone progressions out to  $\underline{\nu} = 3, 14, 23, 24, 25, 17, \text{ and } 3$  have been observed with 457.9 nm, 476.5 nm, 488.0 nm, 514.5 nm, 530.9 nm, 568.2 nm, and 647.1 nm excitation, respectively, for monomeric iodine isolated in an argon matrix. The intensity ratios,  $R_{\underline{\nu}}$  (overtone/fundamental), were determined and plotted versus the laser excitation energy which formed excitation profiles for the overtone. Figure 13 illustrates a plot of the  $R_{\underline{\nu}}$  for the first seven overtones of  $I_2$  in solid argon. The two maxima strongly suggest that the resonance Raman intensity enhancement is due to a resonance coupling of the exciting

radiation with not only the  ${}^3\Pi_{0u}^+ \leftarrow {}^1\Sigma_g^+$  transition, but also with the  ${}^1\Pi_{1u} \leftarrow {}^1\Sigma_g^+$  transition. The dashed curves in Figure 13 represent the intensity ratio curves for the two cases of exact resonance which extrapolate to the two electronic transition energies. Appropriate wavenumbers of the deconvoluted peaks as determined from the MCD spectra of matrix-isolated iodine are  $19,700 \text{ cm}^{-1}$  and  $18,600 \text{ cm}^{-1}$  for the singlet-singlet and singlet-triplet transitions, respectively (61).

RESONANCE RAMAN SPECTRA OF NO<sub>2</sub> and ClO<sub>2</sub>

Resonance Raman spectra have been discussed in previous sections for the anions O<sub>3</sub><sup>-</sup>, Cl<sub>2</sub><sup>-</sup>, and I<sub>2</sub><sup>-</sup>, produced in alkali metal matrix reactions, and the Br<sub>2</sub> and I<sub>2</sub> molecules. The visible absorbing molecules NO<sub>2</sub> and ClO<sub>2</sub> have received extensive gas-phase laser excitation study (16, 18, and references therein), and their laser examination in matrices provides additional means to characterize the role of the matrix in laser-excitation studies. Furthermore, it was heretofore impossible to obtain Raman spectra of NO<sub>2</sub> and ClO<sub>2</sub> because of their intense visible absorption and fluorescence, and the explosive nature of ClO<sub>2</sub>. It was believed that matrix isolation might circumvent these difficulties.

Tevault and Andrews recorded Raman spectra of NO<sub>2</sub> and N<sub>2</sub>O<sub>4</sub> using 4880 Å excitation of a sample of Ar/NO<sub>2</sub> = 100/1 deposited at 16 K (19). The most intense feature in the spectrum was the 262 cm<sup>-1</sup> ν<sub>3</sub> band of N<sub>2</sub>O<sub>4</sub>; the ν<sub>1</sub> and ν<sub>2</sub> bands of N<sub>2</sub>O<sub>4</sub> appeared as weak signals at 1383 and 813 cm<sup>-1</sup>. "Isolated" NO<sub>2</sub> produced equally strong ν<sub>1</sub> and ν<sub>2</sub> signals at 1325 and 752 cm<sup>-1</sup>, respectively. Upon warming the deposited sample to 40 K and re-cooling to 16 K, the NO<sub>2</sub> signals were markedly reduced and the N<sub>2</sub>O<sub>4</sub> signals increased threefold.

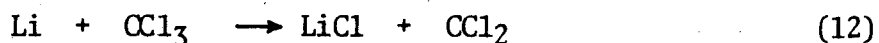
In the overtone region, 2ν<sub>2</sub>, ν<sub>1</sub> + ν<sub>2</sub> and 2ν<sub>1</sub> were observed for <sup>14</sup>NO<sub>2</sub> and <sup>15</sup>NO<sub>2</sub> with lower intensities than the fundamentals; 3ν<sub>2</sub> was also detected for <sup>14</sup>NO<sub>2</sub>. The resonance Raman spectrum of nitrogen dioxide is somewhat unusual in that two strong symmetric fundamentals, ν<sub>1</sub> and ν<sub>2</sub>, and overtones of each were observed along with the combination band ν<sub>1</sub> + ν<sub>2</sub>. No fluorescence was observed in the laser excitation study of matrix-isolated NO<sub>2</sub> (19).

Laser excitation studies of ClO<sub>2</sub> in argon, krypton, xenon, and nitrogen matrices were done with the 4579, 4765, 4880, and 5145 Å argon ion lines (17). The most energetic line, which reaches the electronic absorption of ClO<sub>2</sub>, produced the richest spectrum which is illustrated in Figure 14. The intense resonance Raman progression in the  $\nu_1$  fundamental of ClO<sub>2</sub> is noted with decreasing intensities out to 6  $\nu_1$  along with four series of fluorescence bands labelled a, b, c, and d, which increase in intensity and then decrease in the series. The first a band at 290 cm<sup>-1</sup> is in excellent agreement with the excited state bending frequency  $\nu_2'$ . The a fluorescence series follows the quenching of one quantum of  $\nu_2'$  and gives a progression in  $\nu_1''$ . The a series members were designated ( $\nu_1$ ,0) where  $\nu_1$  is the  $\nu_1$  quantum number. The b series is shifted from a by one quantum of  $\nu_2''$  and its identification follows as ( $\nu_1$ ,1). Likewise, it can be seen that the c and d series involve fluorescence progressions in  $\nu_1$  with higher combinations of  $\nu_2$  which were designated ( $\nu_1$ ,2) and ( $\nu_1$ ,3), respectively.

In the ClO<sub>2</sub> studies where both resonance Raman and fluorescence progressions were observed, the matrix quenches fluorescence and allows the resonance Raman spectrum to be observed (17), which is in marked contrast to the gas phase studies (16).

## FLUORESCENCE STUDIES

While searching unsuccessfully for the Raman spectrum of  $\text{CCl}_3$ , three groups of workers found a broad progression of fluorescence bands arising from  $\text{CCl}_2$  also present in the matrix samples (62,63,64). However, Tevault and Andrews, using the alkali metal matrix reaction to synthesize  $\text{CCl}_2$  by reactions (11) and (12), found that dilution of the samples to one part



reagent per thousand parts matrix gas reduced the series of broad bands and enhanced several series of sharp bands (64). The fluorescence spectra of  $\text{CCl}_2$  at two sample dilutions using 4880 Å excitation are contrasted in Figure 15, which also shows a  $^{13}\text{CCl}_2$  spectrum. The sharp fluorescence bands are due to combination progressions of  $\nu_1''$  and  $\nu_2''$  of  $\text{CCl}_2$ . The values of  $\nu_1''$  for  $\text{CCl}_2$  and  $^{13}\text{CCl}_2$  deduced from the fluorescence spectra are in excellent agreement with infrared measurements of these fundamentals (65). Upon annealing the deposited sample, the sharp series was replaced by the broad series which was attributed to  $\text{CCl}_2$  aggregated with another molecule present in the sample (64).

Similar work with dilute samples of  $\text{CFC1}$  synthesized by the high yield matrix reaction of alkali metal atoms with  $\text{CFC1}_3$  produced 120 resolved bands between 25,000 and 15,000  $\text{cm}^{-1}$  using 3507 and 3564 Å krypton plasma laser excitation. These bands were interpreted as progressions in  $\nu_2''$  of  $\text{CFC1}$  with combinations of  $\nu_1''$  and  $\nu_3''$  emanating from three adjacent vibrational levels in the excited state (66). Again, agreement with the infrared stretching fundamentals (67) was noted. The  $\text{CFC1}$  fluorescence spectrum

produced by the 3640 Å line from a high-pressure mercury arc in these alkali metal studies was similar to the ultraviolet laser-induced spectrum, but as might be expected, two orders of magnitude weaker.

In an alkali metal reaction study with the  $\text{CCl}_2\text{Br}_2$  precursor, the fluorescence spectrum of  $\text{CClBr}$  was excited using the 5682 Å krypton ion laser line (68). Several progressions in  $\nu_2''$  were observed with combination progressions involving  $\nu_1''$  and  $\nu_3''$ , the latter of which matched the direct infrared measurements (69).

Yellow laser excitation of alkali metal- $\text{CBr}_4$  samples produced a fluorescence from 11,500-15,000  $\text{cm}^{-1}$  which consisted of 17 sharp bands spaced 196  $\text{cm}^{-1}$  apart and a weaker series of ten bands with the same spacing but shifted approximately 136  $\text{cm}^{-1}$  lower in energy than the major progression. The two fluorescence series, illustrated in Figure 16, were assigned to progressions in  $\nu_2''$  of  $\text{CBr}_2$  with the weaker series arising from a lower vibronic level by one quantum which provides a measure of  $\nu_2'$  for  $\text{CBr}_2$  of approximately 136  $\text{cm}^{-1}$  (68).

In a particularly interesting vibronic study of matrix isolated PbS, Teichman and Nixon (70) observed fluorescence from three different excited electronic states in the visible region using 5682, 5145, 4880, and 4579 Å laser excitation. The three fluorescence progressions, identified as  $B \rightarrow X$ ,  $A \rightarrow X$ , and  $\underline{a} \rightarrow X$  by comparison to gas phase studies, exhibited average band spacings of 407  $\text{cm}^{-1}$  in close agreement with the 423  $\text{cm}^{-1}$  matrix infrared and Raman value for the PbS fundamental.

Excitation with the 4579 Å line reached the  $\underline{\nu}' = 0$  level of the B state and about  $\underline{\nu}' = 12$  and  $\underline{\nu}' = 30$  in the A and  $\underline{a}$  states. The relative intensities of the  $\underline{a}$  and B emissions were much greater than the A emission.

On the other hand, 4880 and 5145 Å excitation produced a more intense A emission than a emission; however, a strong a emission was observed with 5682 Å excitation. The inference from these observations is that the a and B states are strongly coupled, conceivably by a mechanism involving the matrix, but that coupling between the a or B and A states is weak (70).

Finally, it is appropriate to conclude this review with fluorescence studies of  $C_2^-$  which have shown that vibrational lifetime measurements can be made on matrix-isolated molecules (20). The absorption spectrum of  $C_2^-$  in solid argon has been observed following hydrogen resonance photolysis of  $C_2H_2$  during deposition (71,72). Since the 0-0 transition of  $C_2^-$  in solid argon,  $19,193\text{ cm}^{-1}$ , is near the  $19,430\text{ cm}^{-1}$  argon ion laser line, an intense fluorescence spectrum of  $C_2^-$  was observed (73). Fluorescence progressions including 0-0, 0-1, and 0-2 bands were observed in  $N_2$  and Ar matrices, but of most interest, a second progression containing 1-3, 1-2, 1-1, and 1-0 bands was observed in argon. The 1-0 feature on the blue side of the  $19,430\text{ cm}^{-1}$  exciting line indicates that emission arises from the  $\underline{v}' = 1$  level, apparently reached by secondary excitation of a substantial  $\underline{v}'' = 1$  level population. It was concluded that vibrational relaxation for  $C_2^-$  in solid argon is slow in both ground and excited electronic states (73).

By using an elegant optical double-resonance technique, Allamandola and Nibler have determined vibrational half-lives of 0.2 and 1.2 ms for the  $\underline{v}'' = 1$  and  $\underline{v}'' = 2$  states of argon matrix-isolated  $C_2^-$ , respectively (20). The method employs a pumping laser to populate the 1'' and 2'' states by absorption to 1' and fluorescence to the 1'' and 2'' levels. A tunable probe laser was used to selectively excite 1'' to 0' and the 0' → 0'' fluorescence

markedly increased. By turning off the pumping laser, the decay of the  $0' \rightarrow 0''$  fluorescence gives a measure of the rate of depletion of the  $1''$  level. These successful studies indicate an exciting future for vibrational lifetime measurements of matrix-isolated molecules and the study of vibrational energy transfer phenomena in matrices.

ACKNOWLEDGMENT: This work was supported by the Energy Research and Development Administration, the University of Virginia and the Alfred P. Sloan Foundation.

## REFERENCES

1. L. Andrews, "Infrared and Raman Spectra of Unique-Matrix Isolated Molecules", Vibrational Spectra and Structure, Vol. IV, Elsevier Scientific Publishing Co., Amsterdam, 1975.
2. J. S. Shirk and H. H. Claassen, *J. Chem. Phys.* 54, 3237 (1971).
3. G. A. Ozin, "Matrix Isolation Laser Raman Spectroscopy", Vibrational Spectroscopy of Trapped Species, ed., H. E. Hallam, John Wiley and Sons, London, 1973.
4. J. W. Nibler, *Advances in Laser Raman Spectroscopy* 1, 70 (1972).
5. D. A. Hatzenbuehler and L. Andrews, *J. Chem. Phys.* 56, 3398 (1972).
6. J. W. Nibler and D. A. Coe, *J. Chem. Phys.* 55, 5134 (1971).
7. G. A. Ozin and A. Van der Voet, *J. Chem. Phys.* 56, 4768 (1972).
8. L. Andrews and R. C. Spiker, Jr., *J. Chem. Phys.* 59, 1863 (1973).
9. L. Andrews, *J. Chem. Phys.* 57, 51 (1972).
10. L. Andrews and R. R. Smardzewski, *J. Chem. Phys.* 58, 2258 (1973).
11. F. K. Chi and L. Andrews, *J. Phys. Chem.* 77, 3062 (1973).
12. L. Andrews and R. C. Spiker, Jr., *J. Phys. Chem.* 76, 3208 (1972).
13. W. F. Howard, Jr. and L. Andrews, *J. Amer. Chem. Soc.* 96, 7864 (1974).
14. J. B. Bates, M. H. Brooker, and G. E. Boyd, *Chem. Phys. Lett.* 16, 391 (1972).
15. W. F. Howard, Jr. and L. Andrews, *J. Amer. Chem. Soc.* 97, May (1975).
16. R. F. Curl, Jr., K. Abe, J. Bissinger, C. Bennett, and F. K. Tittel, *J. Mol. Spectrosc.* 48, 72 (1973).
17. F. K. Chi and L. Andrews, *J. Mol. Spectrosc.* 52, 82 (1974).
18. K. Abe, F. Myers, T. K. McCubbin, S. R. Polo, *J. Mol. Spectrosc.* 38, 552 (1971).

Ref. contd.

19. D. E. Tevault and L. Andrews, *Spectrochim. Acta* 30A, 969 (1974).
20. L. J. Allamandola and J. W. Nibler, *Chem. Phys. Lett.* 28, 335 (1974).
21. D. E. Tevault and L. Andrews, *J. Mol. Spectrosc.* 54, 110 (1975).
22. L. Andrews, *J. Chem. Phys.* 50, 4288 (1969).
23. D. W. Smith and L. Andrews, *J. Chem. Phys.* 60, 81 (1974).
24. L. Andrews, *J. Phys. Chem.* 73, 3922 (1969).
25. L. Andrews, *J. Chem. Phys.* 54, 4935 (1971).
26. L. Andrews, J. T. Hwang, and C. Trindle, *J. Phys. Chem.* 77, 1065 (1973).
27. R. R. Smardzewski and L. Andrews, *J. Chem. Phys.* 57, 1327 (1972).
28. R. R. Smardzewski and L. Andrews, *J. Phys. Chem.* 77, 801 (1973).
29. M. E. Jacox and D. E. Milligan, *Chem. Phys. Lett.* 14, 518 (1972).
30. R. C. Spiker, Jr. and L. Andrews, *J. Chem. Phys.* 59, 1851 (1973).
31. M. E. Jacox and D. E. Milligan, *J. Mol. Spectrosc.* 43, 148 (1972).
32. L. Andrews, "Optical Spectra of the Ozonide Ion in the Matrix Isolated  $M^+O_3^-$  Species", to be published.
33. J. B. Bates and J. C. Pigg, *J. Chem. Phys.* 63, XXXX (1975).
34. L. Andrews, unpublished results (1971).
35. W. F. Howard, Jr. and L. Andrews, *J. Amer. Chem. Soc.* 95, 3045 (1973).
36. W. F. Howard, Jr. and L. Andrews, *Inorg. Chem.* \_\_, XXXX (1975).
37. L. Andrews, "Optical Spectra of Alkali Metal-Halogen Matrix Reaction Products", to be published.
38. R. K. Steunenberg and R. C. Vogel, *J. Amer. Chem. Soc.* 78, 901 (1956).
39. W. F. Howard, Jr. and L. Andrews, *J. Amer. Chem. Soc.* 95, 2056 (1973).
40. W. F. Howard, Jr. and L. Andrews, *Inorg. Chem.* \_\_, XXXX (1975).

Ref. contd.

41. B. S. Ault and L. Andrews, to be published.
42. W. Gabes and D. J. Stufkens, *Spectrochim. Acta* 30A, 1835 (1974).
43. W. Kiefer and H. J. Bernstein, *Chem. Phys. Lett.* 16, 5(1972) and W. Kiefer, *Applied Spectrosc.* 28, 115 (1974).
44. A. Arkell, R. R. Reinhard and L. P. Larson, *J. Amer. Chem. Soc.* 87, 1016 (1965).
45. L. Andrews and J. I. Raymond, *J. Chem. Phys.* 55, 3078 (1971).
46. A. Glissman and H. J. Schumacher, *Zeit. Phys. Chem.* B24, 328 (1934).
47. F. K. Chi and L. Andrews, *J. Phys. Chem.* 77, 3062 (1973).
48. M. M. Rochkind and G. C. Pimentel, *J. Chem. Phys.* 46, 4481 (1967).
49. M. Basco and R. D. Morse, *J. Mol. Spectrosc.* 45, 35 (1973).
50. J. J. Turner and G. C. Pimentel, Noble-Gas Compounds, ed. H. H. Hyman, University of Chicago Press, Chicago, 1963.
51. L. Y. Nelson and G. C. Pimentel, *Inorg. Chem.* 6, 1758 (1967).
52. D. Boal and G. A. Ozin, *Spectrosc. Lett.* 4, 43 (1971).
53. W. F. Howard, Jr. and L. Andrews, *J. Amer. Chem. Soc.* 96, 7864 (1974).
54. I. R. Beattie and A. German, to be published.
55. V. E. Bondybey, Ph.D Thesis, University of California, Berkeley, 1971, and G. C. Pimentel, personal communication, 1974.
56. W. F. Howard, Jr., M. S. Thesis, University of Virginia, Charlottesville, Virginia, 1974.
57. B. S. Ault, W. F. Howard, Jr., and L. Andrews, *J. Mol. Spectrosc.* 54, March (1975).
58. W. F. Howard, Jr. and L. Andrews, *J. Raman. Spectrosc.*, in press.

Ref. contd.

59. J. M. Grzybowski and L. Andrews, *J. Raman Spectrosc.*, in press.
60. B. S. Ault and L. Andrews, to be published.
61. J. Jasinski and P. Schatz, unpublished results (1974).
62. J. S. Shirk, *J. Chem. Phys.* 55, 3608 (1971).
63. J. W. Nibler, unpublished work (1972).
64. D. E. Tevault and L. Andrews, *J. Mol. Spectrosc.* 54, 110 (1975).
65. L. Andrews, *J. Chem. Phys.* 48, 979 (1968).
66. D. E. Tevault and L. Andrews, *J. Mol. Spectrosc.* 54, 54 (1975).
67. C. E. Smith, D. E. Milligan, and M. E. Jacox, *J. Chem. Phys.* 54, 2780 (1971).
68. D. E. Tevault and L. Andrews, *J. Amer. Chem. Soc.* 97, April (1975).
69. L. Andrews and T. G. Carver, *J. Chem. Phys.* 49, 896 (1968).
70. R. A. Teichman III and E. R. Nixon, *J. Mol. Spectrosc.* 54, 78 (1975).
71. D. E. Milligan, M. E. Jacox and L. Abouaf-Marguin, *J. Chem. Phys.* 46, 4562 (1967) and 51, 1952 (1969).
72. W. R. M. Graham, K. I. Dismuke, and W. Weltner, Jr., *J. Chem. Phys.* 61, 4793 (1974).
73. V. Bondybey and J. W. Nibler, *J. Chem. Phys.* 56, 4719 (1972).

## FIGURE CAPTIONS

- Fig. 1. Infrared and Raman spectra of lithium superoxide,  $\text{Li}^+\text{O}_2^-$  using lithium-7 and 30%  $^{18}\text{O}_2$ , 50%  $^{16}\text{O}^{18}\text{O}$ , 20%  $^{16}\text{O}_2$  at concentrations of  $\text{Ar}/\text{O}_2 = 100$ . Raman spectrum recorded using 200 mW of 4880 Å excitation and long wavelength pass dielectric filter in  $1000\text{ cm}^{-1}$  region.
- Fig. 2. Raman spectrum of argon matrix-isolated sodium ozonide using 200 mW of 5145 Å excitation. (Reprinted from Ref.(8), by courtesy of the American Institute of Physics).
- Fig. 3. Raman spectra of argon matrix-isolated sodium ozonide using different exciting wavelengths.  $\text{Ar}/\text{O}_3 = 100$ . (Reprinted from Ref.(8), by courtesy of the American Institute of Physics).
- Fig. 4. Raman spectra of  $\text{F}_2$  and  $\text{Cl}_2$  matrix reactions with Na atoms. Parameters:  $\text{Ar}/\text{F}_2 = 50/1$ , 45 mW of 4880 Å excitation,  $0.1 \times 10^{-9}$  Å range;  $\text{Ar}/\text{F}_2/\text{Cl}_2 = 400/3/1$ , 250 mW of 5145 Å excitation,  $0.1 \times 10^{-9}$  Å range;  $\text{Ar}/\text{Cl}_2 = 100/1$ , 150 mW of 4880 Å excitation,  $0.3 \times 10^{-9}$  Å range. All scan speeds  $20\text{ cm}^{-1}/\text{min}$ . (Reprinted from Ref.(36), by courtesy of the American Chemical Society).
- Fig. 5. Raman spectra of alkali metal-chlorine matrix reaction products. P denotes the  $\text{Cl}_2$  precursor signal. Parameters:  $0.3 \times 10^{-9}$  Å range, 3 sec rise time,  $20\text{ cm}^{-1}/\text{min}$  scan speed. Li, Na, K used 150 mW of 4880 Å excitation, Rb used 75 mW of 4765 Å and Cs used 600 mW of 4579 Å excitation. (Reprinted from Ref.(40), by courtesy of the American Chemical Society).

Fig. Cap. contd.

- Fig. 6. Resonance Raman spectrum of argon matrix-isolated  $\text{Cs}^+\text{Cl}_2^-$  at 16 K. Note resolution of  $^{35}\text{Cl}_2^-$  and  $^{35}\text{Cl}^{37}\text{Cl}^-$  splittings in overtones. Parameters: 75 mW of 4579 Å excitation,  $20\text{ cm}^{-1}/\text{min}$  scan speed, (A)  $0.3 \times 10^{-9}$  Å range, 3 sec rise time, (B)  $0.1 \times 10^{-9}$  Å range, 10 sec rise time. (Reprinted from Ref.(40), by courtesy of the American Chemical Society).
- Fig. 7. Resonance Raman spectra of  $\text{Cs}^+\text{Cl}_2^-$  as a function of laser excitation wavelength. 5145 and 4880 Å, 150 mW; 4765 Å, 100 mW; 4579 Å, 75 mW at sample. (Reprinted from Ref.(40), by courtesy of the American Chemical Society).
- Fig. 8. Raman spectra from  $300\text{-}1100\text{ cm}^{-1}$  for oxygen difluoride in solid argon at 16 K using 4880 Å excitation,  $\text{Ar}/\text{OF}_2 = 100$ . Spectrum(a) initial spectrum recorded, arrows denote region of spectrum scanned after indicated time of exposure to the 4880 Å laser line. Spectrum (b) sample deposited for four hours with simultaneous 4880 Å photolysis for the last three hours, initial spectrum recorded. (Reprinted from Ref.(9), by courtesy of the American Institute of Physics).
- Fig. 9. Infrared and Raman spectra of  $\text{Cl}_2\text{O}$  and its photolysis products.  $\text{Ar}/\text{Cl}_2\text{O} = 100$ . Infrared spectrum recorded after 10 min of ultraviolet photolysis. Raman spectrum recorded with 300 mW of 4880 Å excitation.
- Fig. 10. Raman spectra produced by laser excitation of noble-gas halogen mixtures at 16 K. 30-50 mW of 4880 Å light at the sample.  $1 \times 10^{-9}$  Å range for  $\text{Xe}:\text{F}_2$  and  $0.1 \times 10^{-9}$  Å range for others. continued...

Fig. Cap. contd.

Fig. 10. Inset  $242\text{ cm}^{-1}$  band marked with an asterisk in Kr:Cl<sub>2</sub> spectrum contd.

was produced by microwave discharge, not by laser photolysis.

(Reprinted from Ref. (53), by courtesy of the American Chemical Society).

Fig. 11. Infrared and Raman spectra of photolysed Xe:ClF samples with Raman spectrum of Xe:F<sub>2</sub>:Cl<sub>2</sub> shown for comparison. The infrared study used blue mercury-arc photolysis; Raman studies employed 30-40 mW of laser power at the sample. (Reprinted from Ref. (53), by courtesy of the American Chemical Society).

Fig. 12. Resonance Raman spectra of iodine as a function of concentration in argon matrices.  $5145\text{ \AA}$  excitation and  $50\text{ cm}^{-1}/\text{min}$  scan speed for all spectra. Ar/I<sub>2</sub> = 2500 and 1000, 125-150 mW laser power and  $0.1 \times 10^{-9}\text{ A}$  range. Ar/I<sub>2</sub> = 400/1 (low region) 15 mW,  $0.1 \times 10^{-9}\text{ A}$  range; (high region) 150 mW  $0.3 \times 10^{-9}\text{ A}$  range. (Reprinted from Ref. (58), by courtesy of D. Reidel Publishing Co.).

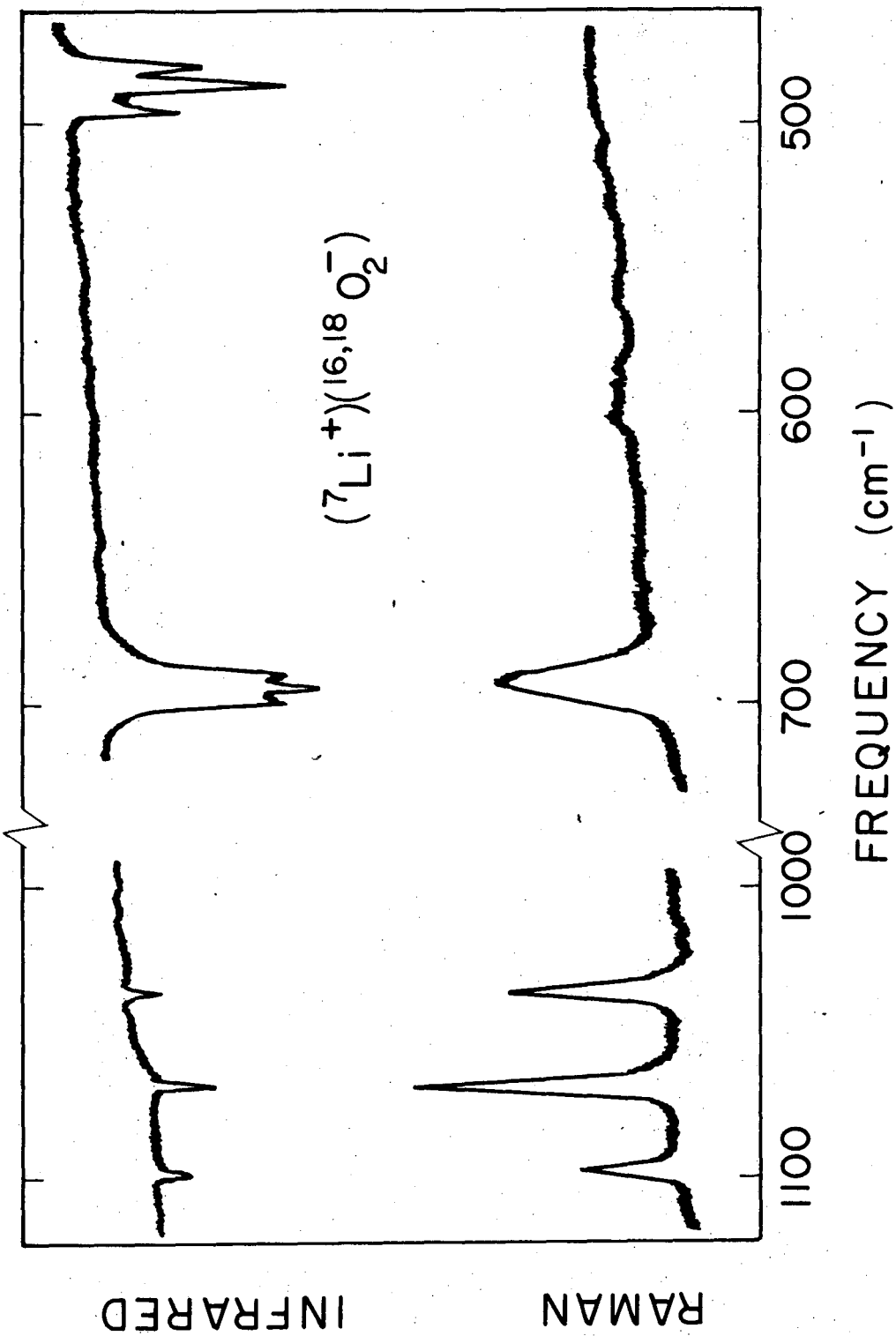
Fig. 13. Resonance Raman excitation profiles for the first seven overtones of argon matrix isolated monomeric I<sub>2</sub>. The broken curves represent intensity ratio curves for the two cases of exact resonance. (Reprinted from Ref. (59), by courtesy of D. Reidel Publishing Co.).

Fig. 14. Laser excitation spectrum of argon matrix-isolated chlorine dioxide, Ar/ClO<sub>2</sub> = 150, using 200 mW of  $4579\text{ \AA}$  light. Resonance Raman progression in  $\nu_1$  of ClO<sub>2</sub> labelled  $n\nu_1$ . Fluorescence bands labelled a, b, c, and d. (Reprinted from Ref. (17), by courtesy Academic Press, Inc.).

Fig. Cap. contd.

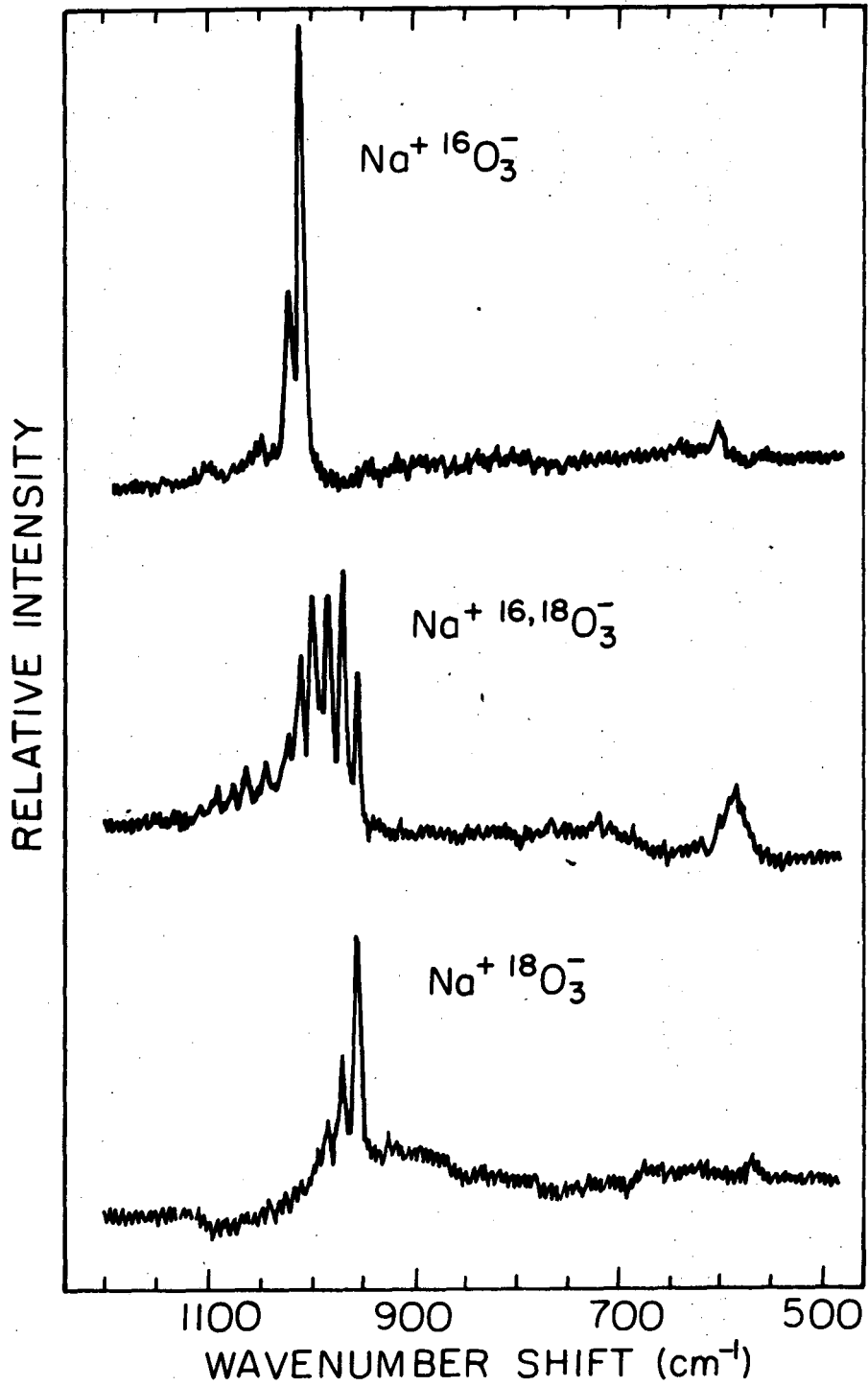
Fig. 15. High-resolution fluorescence spectra of samples produced by the co-deposition of alkali metal atoms and  $\text{CCl}_4$  diluted in argon using  $4880 \text{ \AA}$  laser excitation. Top spectrum shows broad bands common to more concentrated samples. The two bottom spectra contrast dilute carbon isotopic samples. Dashed lines show that sharp bands in the concentrated sample coincide with bands in the middle spectrum and indicate the isotopic shifts of the a and d progressions. Broken line shows the coincidence of the isotopic broad band spectra which were also observed in the  $^{13}\text{CCl}_4$  experiment. (Reprinted from Ref. (21), by courtesy of Academic Press, Inc.).

Fig. 16. Fluorescence spectrum of  $\text{CBr}_2$  produced by  $5682 \text{ \AA}$  excitation of a matrix prepared by codepositing Na atoms with an  $\text{Ar}/\text{CBr}_4 = 1000/1$  gas mixture on a copper wedge at 12 K. (Reprinted from Ref. (68), by courtesy of the American Chemical Society).



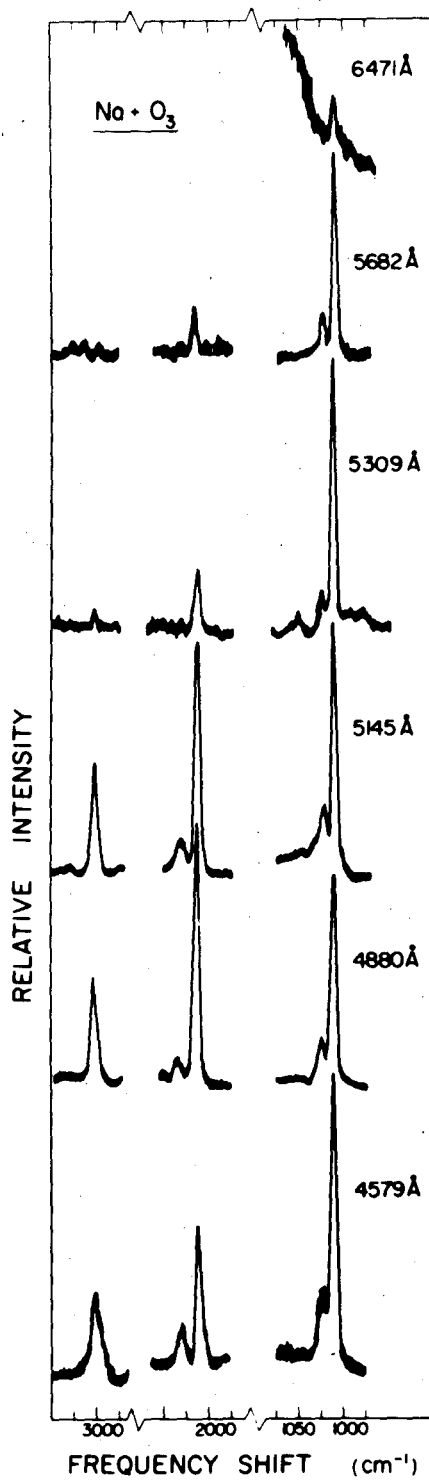
XBL 753-734

Figure 1



XBL 753 - 5985

Figure 2



XBL 754-6122

Figure 3

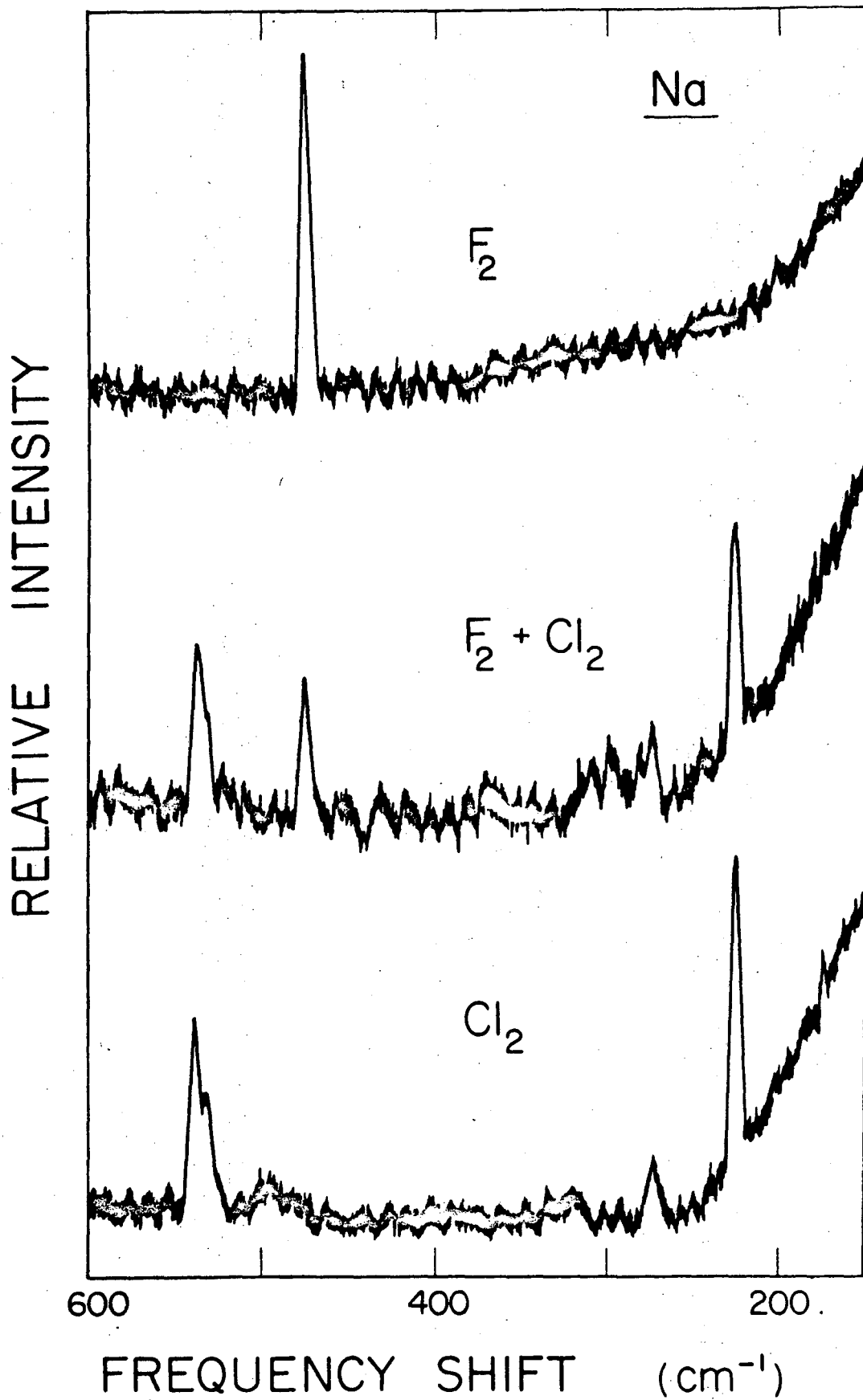


Figure 4

-47-

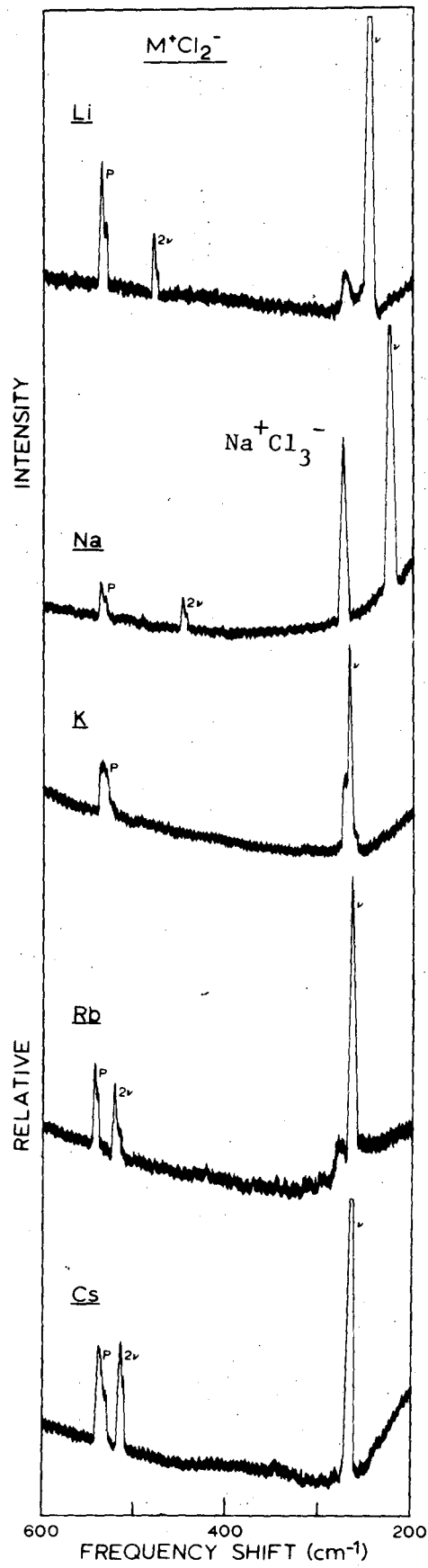
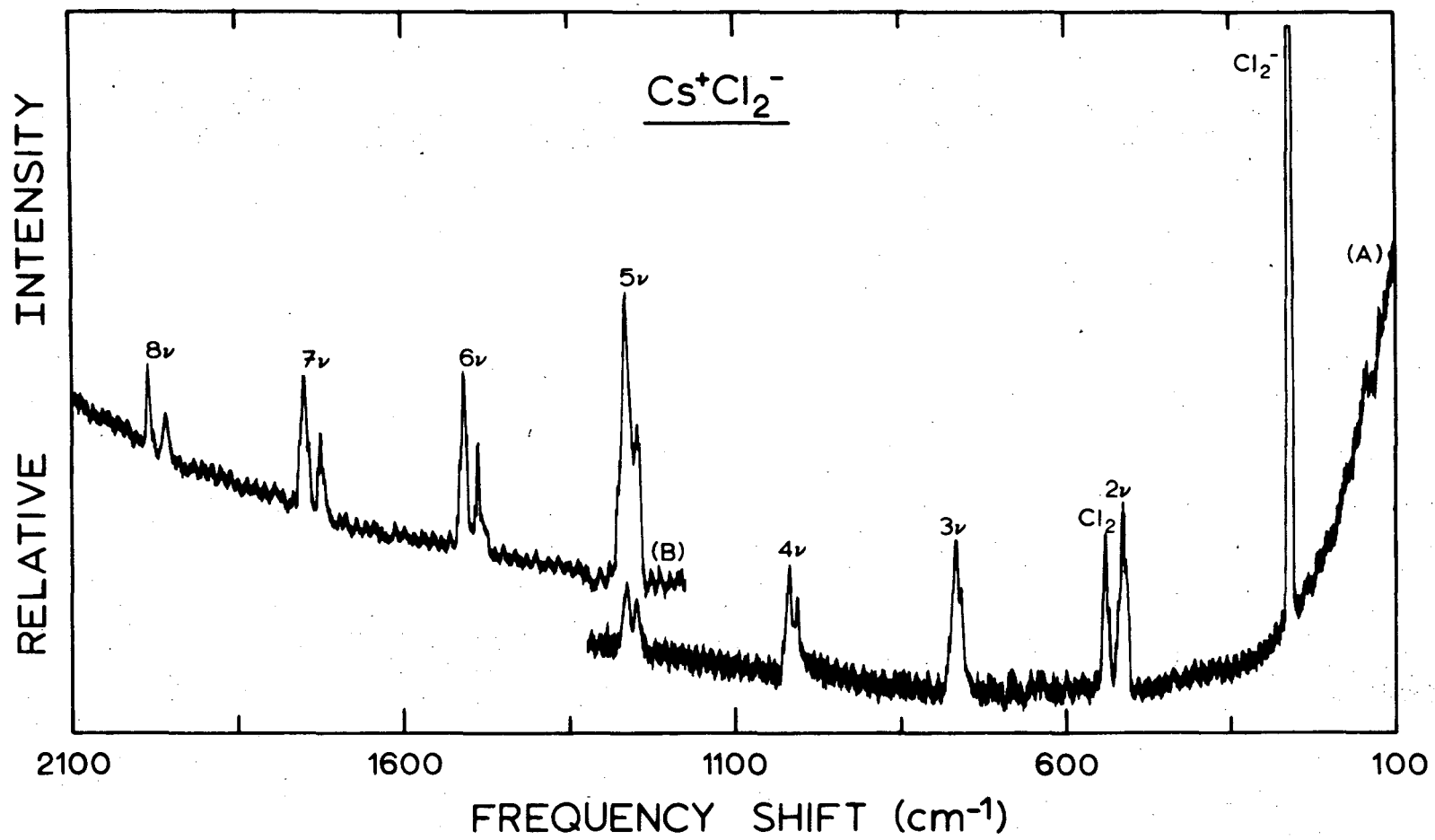


Figure 5

Figure 6



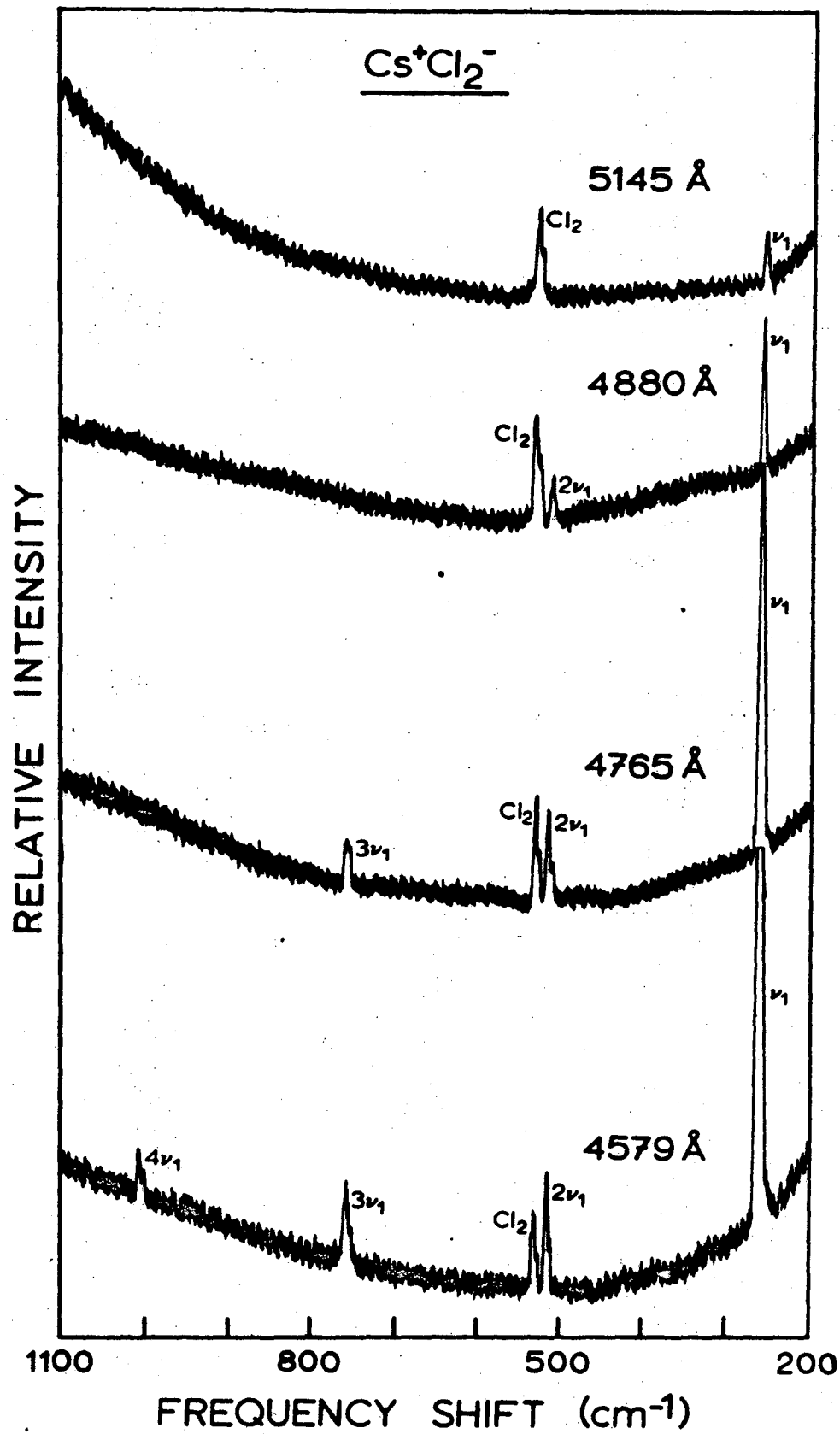


Figure 7

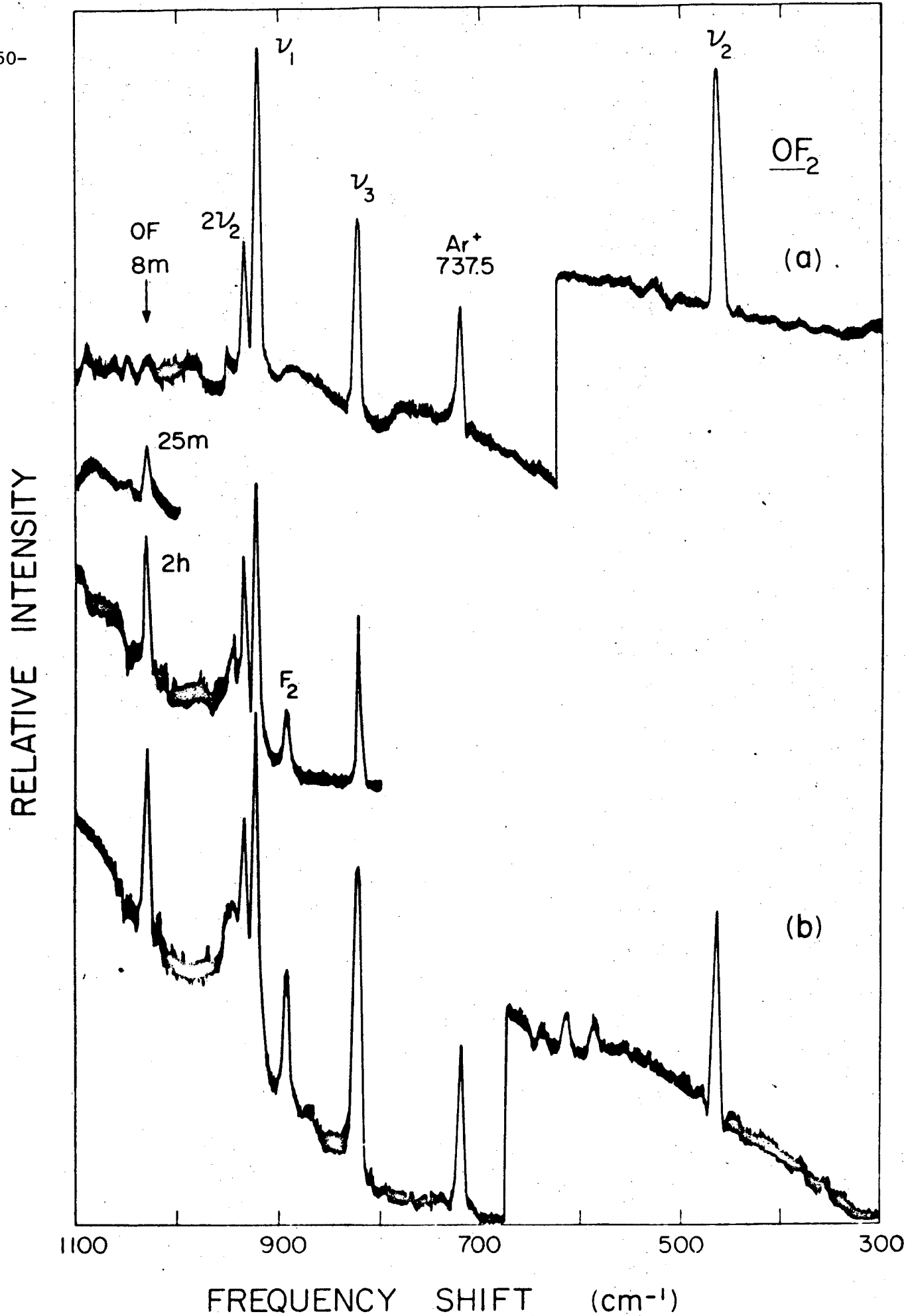
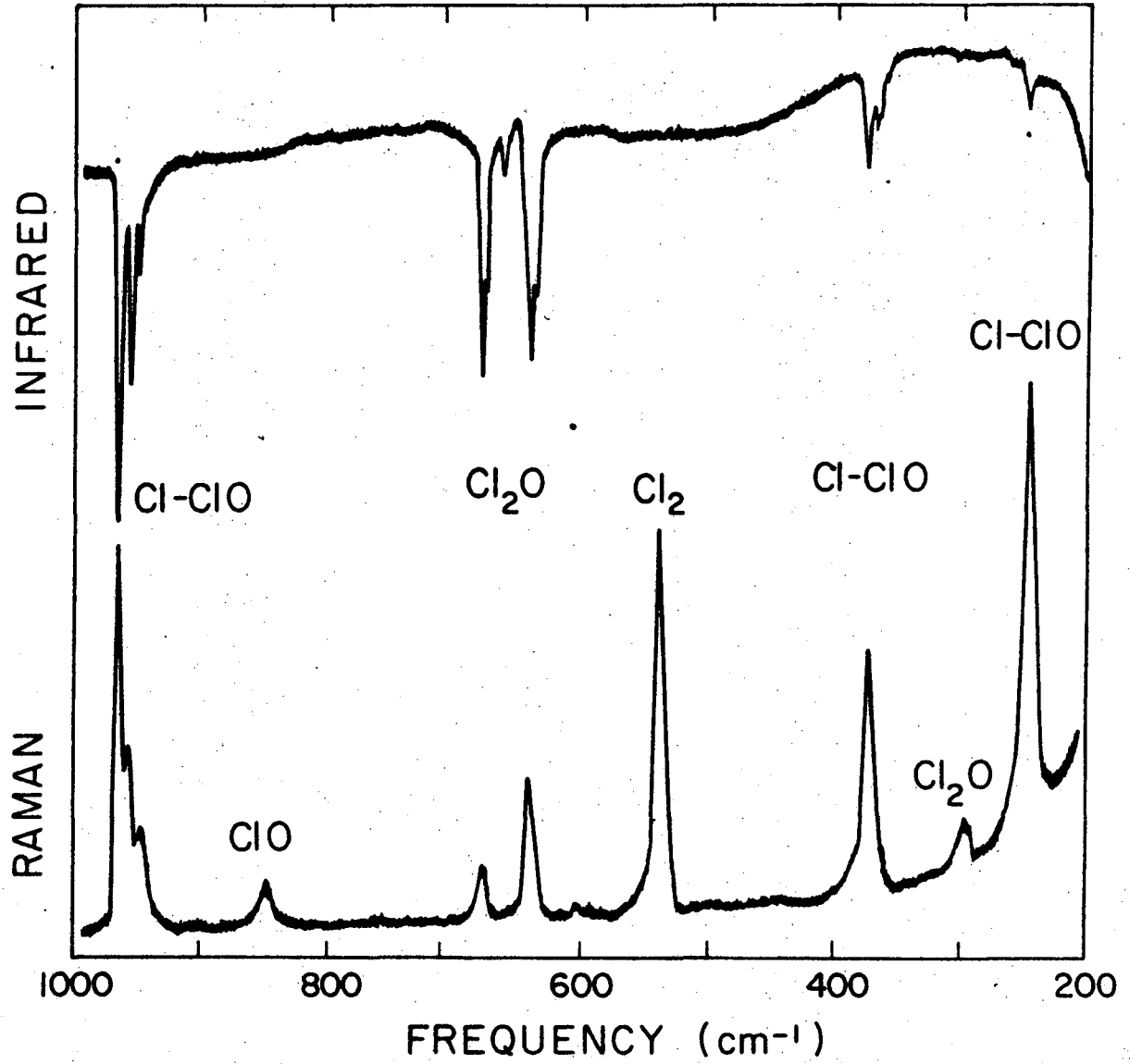


Figure 8



XBL 753-733

Figure 9

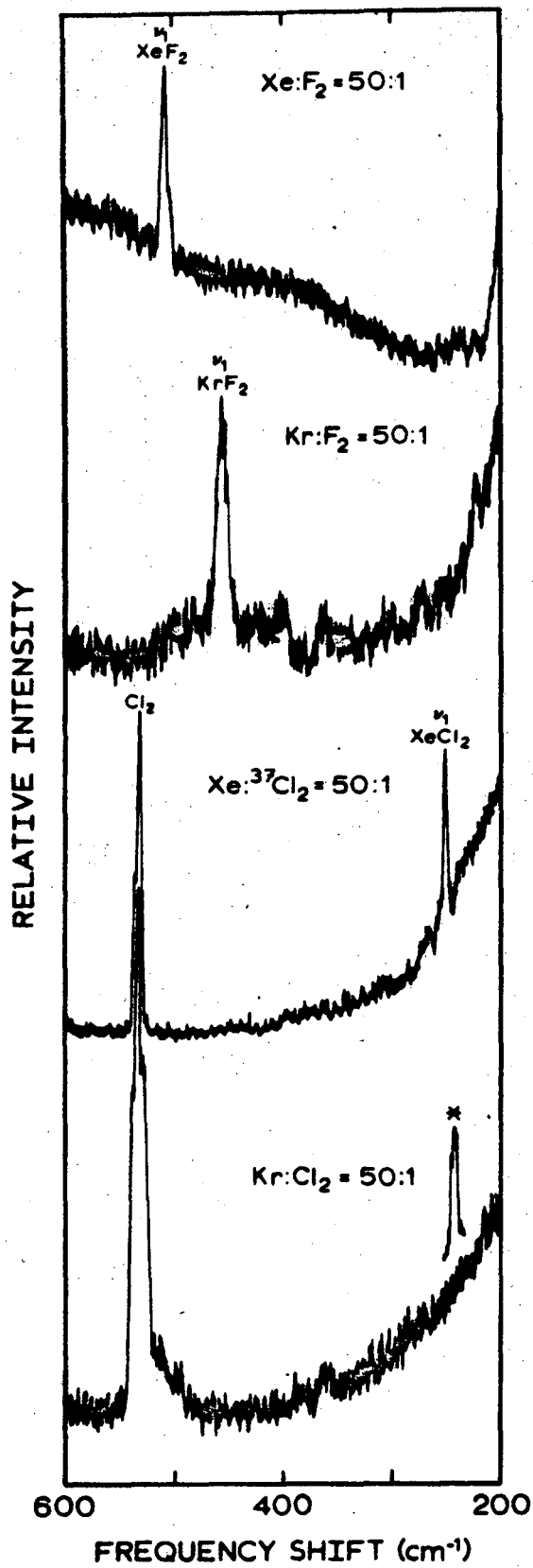


Figure 10

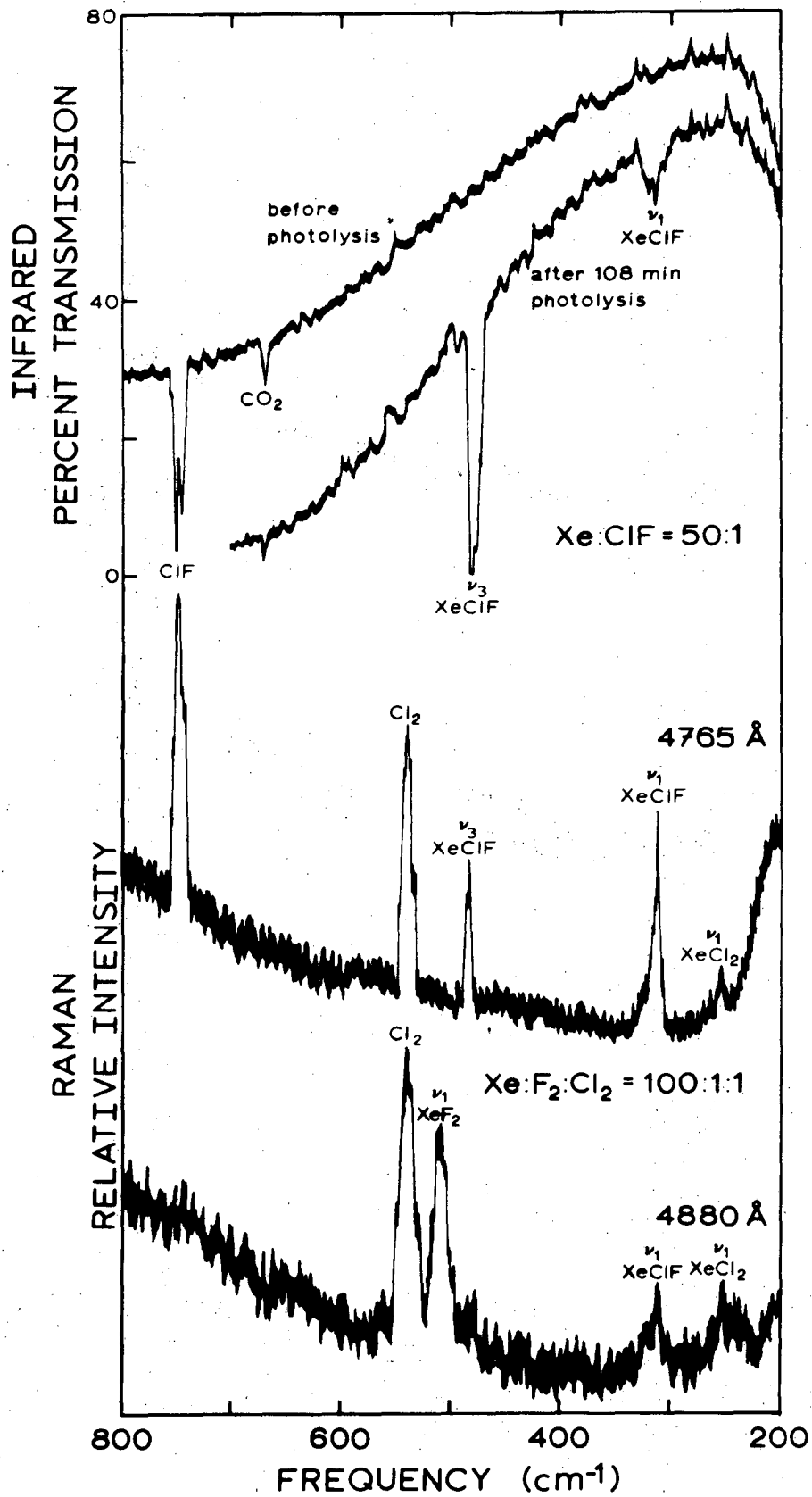


Figure 11

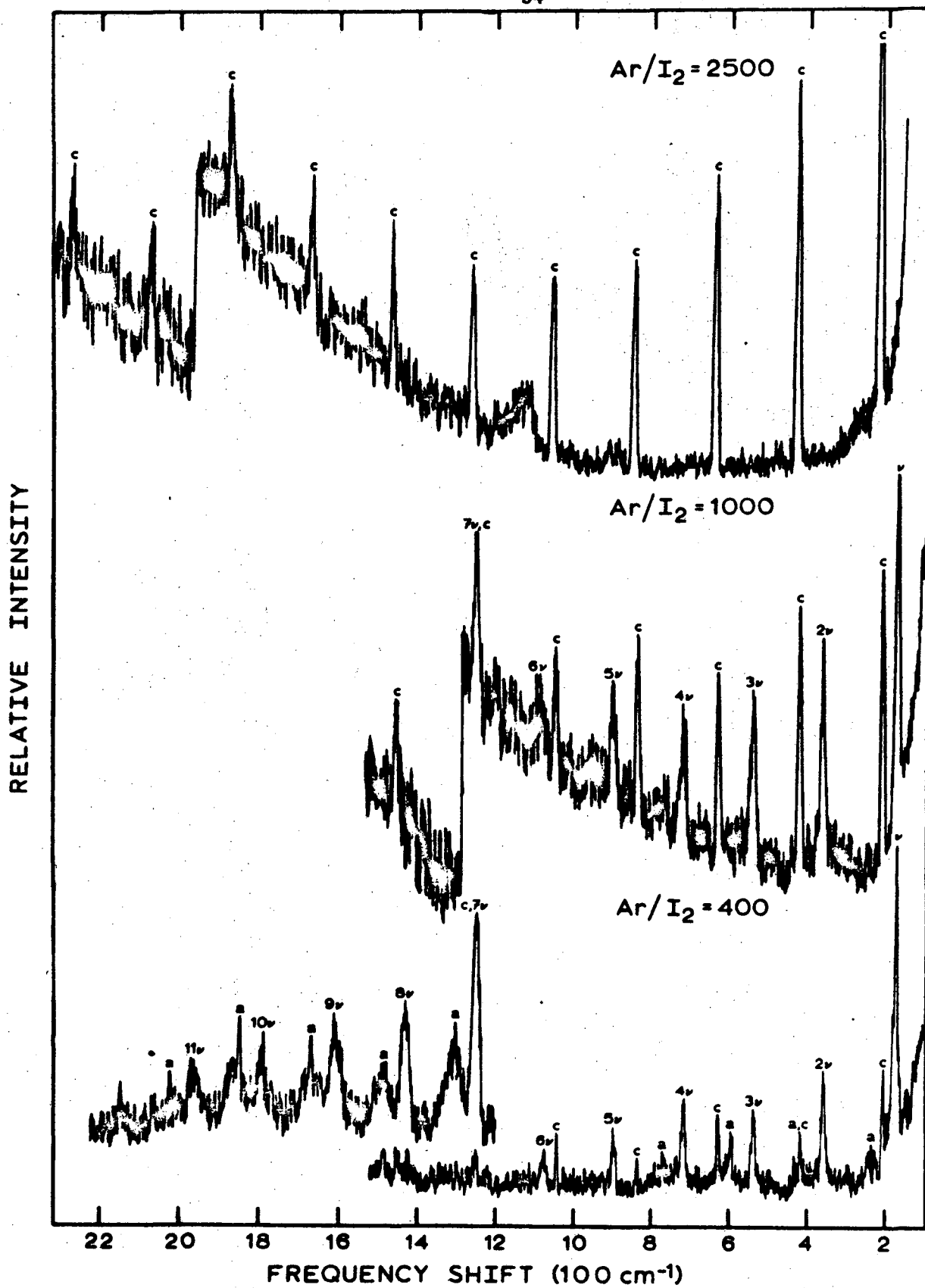
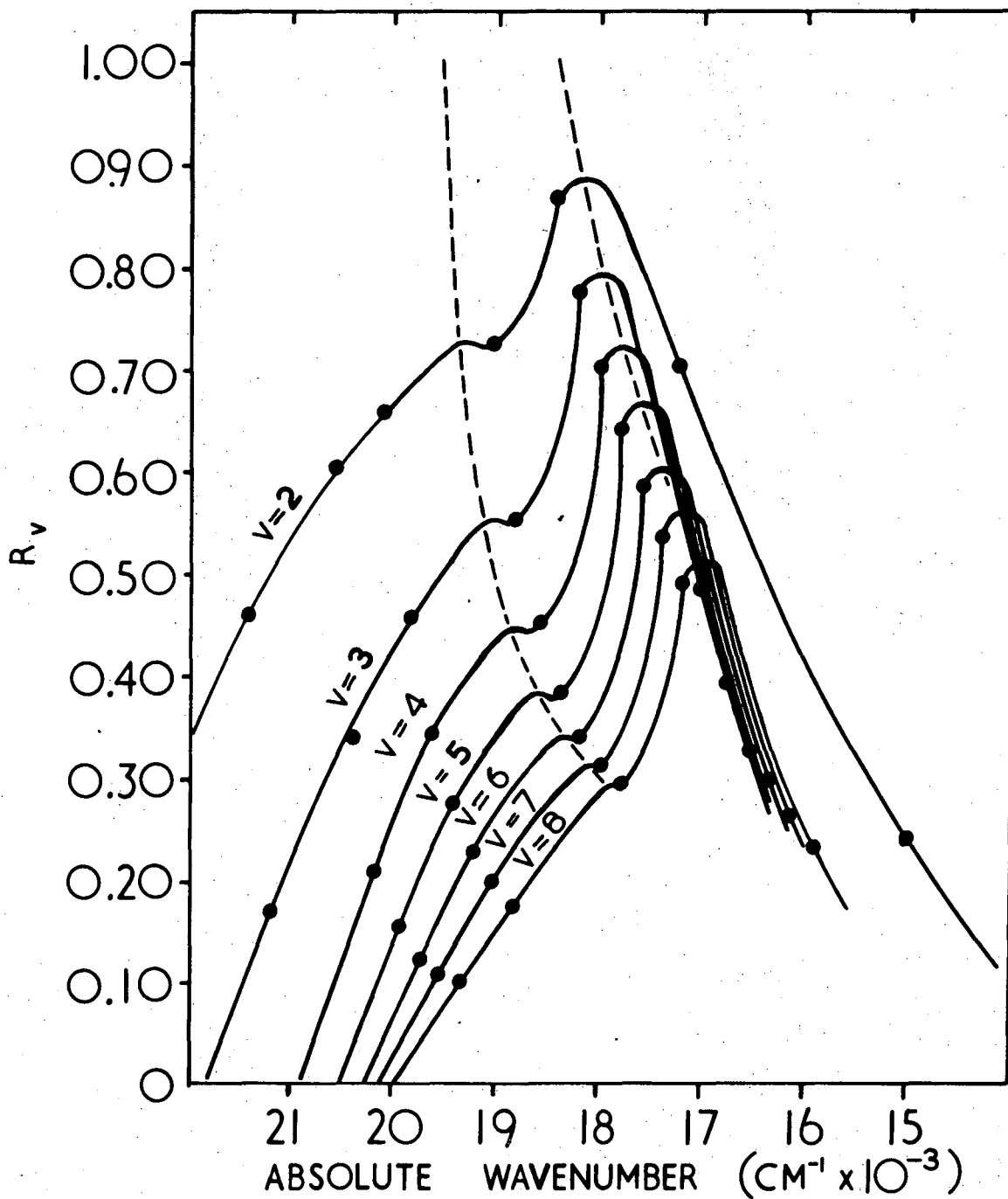


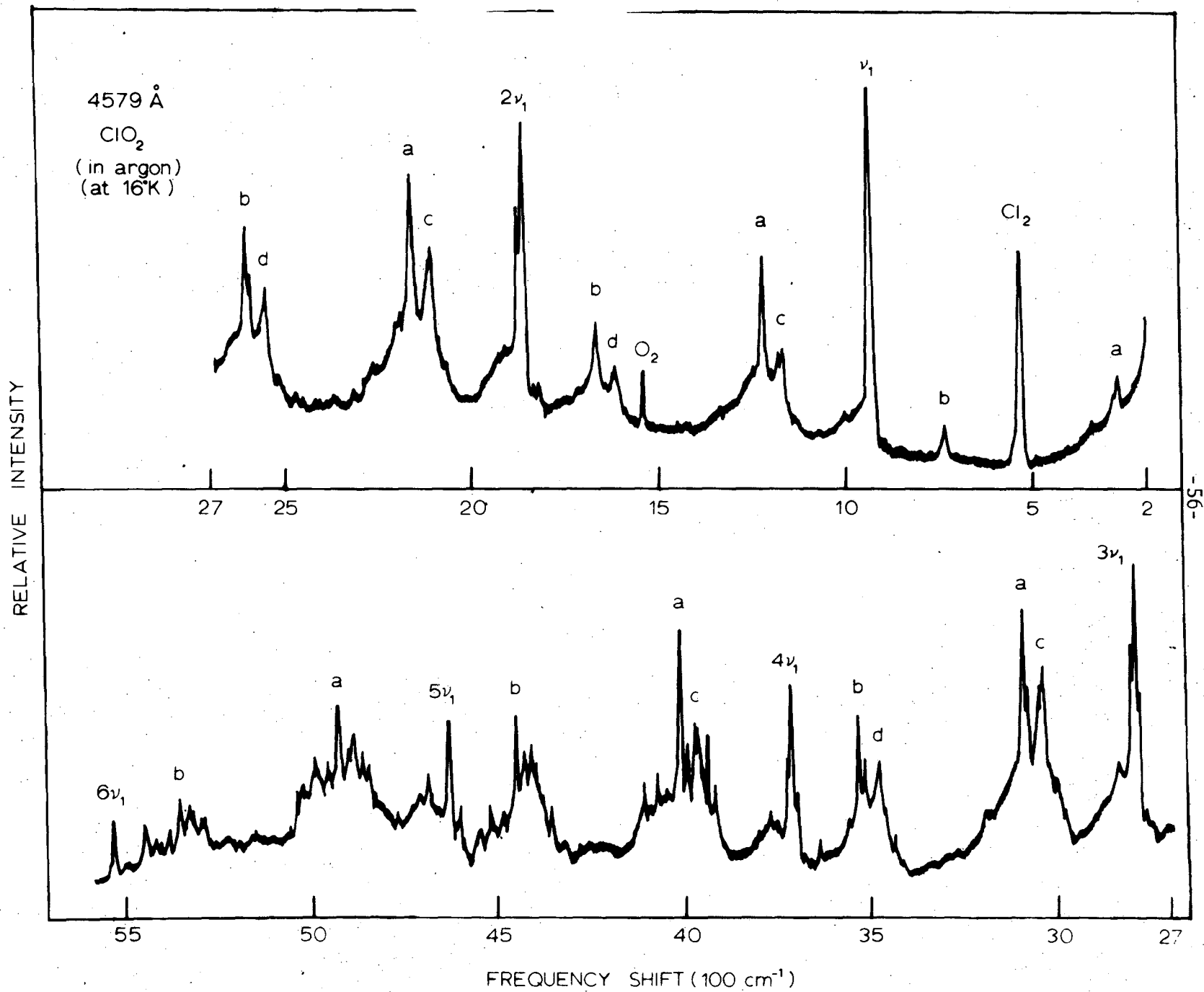
Figure 12



XBL 753-732

Figure 13

Figure 14



00004302891

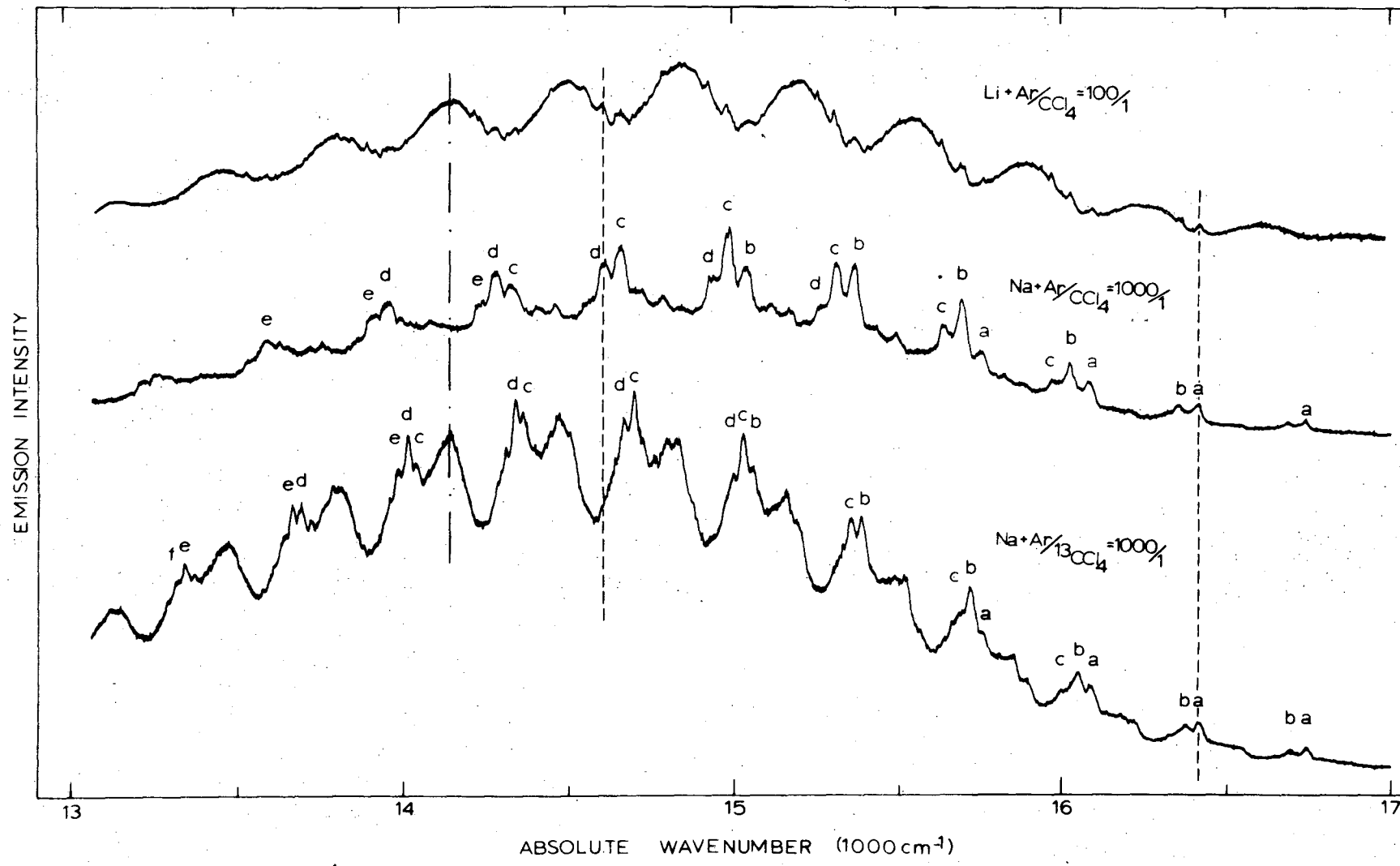


Figure 15

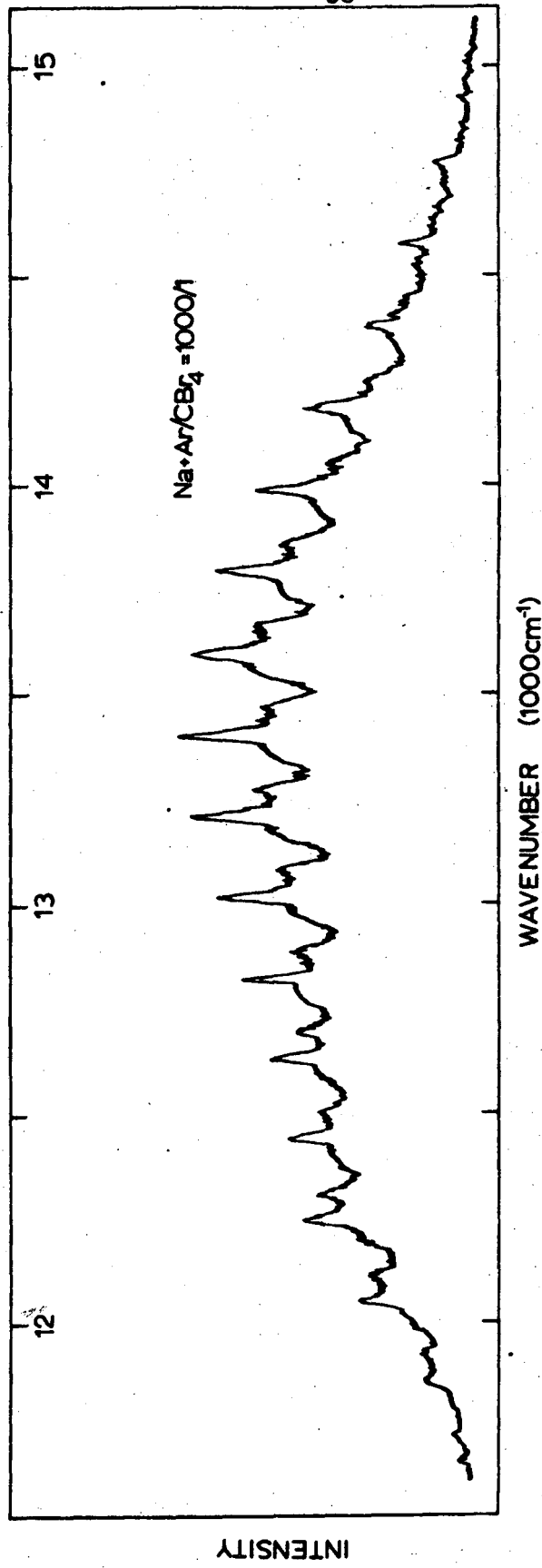


Figure 16

**LEGAL NOTICE**

*This report was prepared as an account of work sponsored by the United States Government. Neither the United States nor the United States Energy Research and Development Administration, nor any of their employees, nor any of their contractors, subcontractors, or their employees, makes any warranty, express or implied, or assumes any legal liability or responsibility for the accuracy, completeness or usefulness of any information, apparatus, product or process disclosed, or represents that its use would not infringe privately owned rights.*

TECHNICAL INFORMATION DIVISION  
LAWRENCE BERKELEY LABORATORY  
UNIVERSITY OF CALIFORNIA  
BERKELEY, CALIFORNIA 94720